CONVERSION OF MIXALCO PROCESS SLUDGE TO LIQUID TRANSPORTATION FUELS

A Dissertation

by

ELIASU AZINYUI TEISEH

Submitted to the Office of Graduate Studies of
Texas A&M University
in partial fulfillment of the requirements for the degree of

DOCTOR OF PHILOSOPHY

May 2012

Major Subject: Biological and Agricultural Engineering

Conversion of MixAlco Process Sludge to Liquid Transportation Fuels

CONVERSION OF MIXALCO PROCESS SLUDGE TO LIQUID TRANSPORTATION FUELS

A Dissertation

by

ELIASU AZINYUI TEISEH

Submitted to the Office of Graduate Studies of
Texas A&M University
in partial fulfillment of the requirements for the degree of

DOCTOR OF PHILOSOPHY

Approved by:

Chair of Committee,	Sergio Capareda
Committee Members,	James Holste
	Raghupathy Karthikeyan
	Sandum Fernando
Department Head,	Stephen Searcy

May 2012

Major Subject: Biological and Agricultural Engineering

ABSTRACT

Conversion of MixAlco Process Sludge to Liquid Transportation Fuels. (May 2012)
Eliasu Azinyui Teiseh, B.S., University of Buea;
M.S., University of Wyoming
Chair of Advisory Committee: Dr. Sergio Capareda

About 8 tons of dry undigested solid waste is generated by the MixAlco process for every 40 tons of food residue waste fed into the process. This MixAlco process produces liquid fuels and the sludge generated can be further converted into synthesis gas using the process of pyrolysis. The hydrogen component of the product synthesis gas may be separated by pressure swing adsorption and used in the hydrogenation of ketones into fuels and chemicals. The synthesis gas may also be catalytically converted into liquid fuels via the Fischer-Tropsch synthesis process.

The auger-type pyrolyzer was operated at a temperature between 630-770 ^{o}C and at feed rates in the range of 280-374 g/minute. The response surface statistical method was used to obtain the highest syngas composition of 43.9±3.36 v % H_2/33.3±3.29 v % CO at 740 ^{o}C. The CH_4 concentration was 20.3±2.99 v %. For every ton of sludge pyrolyzed, 5,990 g H_2 (719.3 MJ), 65,000 g CO (660 MJ) and 21,170 g CH_4 (1055.4 MJ) were projected to be produced at optimum condition. At all temperatures, the sum of the energies of the products was greater than the electrical energy needed to sustain the process, making it energy neutral.

To generate internal H_2 for the MixAlco process, a method was developed to efficiently separate H_2 using pressure swing adsorption (PSA) from the synthesis gas, with activated carbon and molecular sieve 5Å as adsorbents. The H_2 can be used to hydrogenate ketones generated from the MixAlco process to more liquid fuels. Breakthrough curves, cycle mass balances and cycle bed productivities (CBP) were used to determine the maximum hydrogen CBP using different adsorbent amounts at a synthesis gas feed rate of 10 standard lpm and pressure of 118 atm. A 99.9 % H_2 purity

was obtained. After a maximum CBP of 66 % was obtained further increases in % recovery led to a decrease in CBP.

The synthesis gas can also be catalytically converted into liquid fuels by the Fischer-Tropsch synthesis (FTS) process. A Co-SiO_2/Mo-Pd-Pt-ZSM-5 catalyst with a metal-metal-acid functionality was synthesized with the aim of increasing the selectivity of JP-8 (C_{10}-C_{17}) fuel range. The specific surface areas of the two catalysts were characterized using the BET technique. The electron probe microanalyzer (with WDS and EDS capabilities) was then used to confirm the presence of the applied metals Co, Mo, Pd and Pt on the respective supports. In addition to the gasoline (C_4-C_{12}) also produced, the synthesis gas H_2:CO ratio was also adjusted to 1.90 for optimum cobalt performance in an enhanced FTS process. At 10 atm (150 psig) and 250 ^oC, the conventional FTS catalyst Co-SiO_2 produced fuels rich in hydrocarbons within the gasoline carbon number range. At the same conditions the Co-SiO_2-Mo-Pd-Pt/HZSM-5 catalyst increased the selectivity of JP-8. When Co-SiO_2/Mo-Pd-Pt-HZSM-5 was used at 13.6 atm (200 psig) and 250 ^oC, a further increase in the selectivity of JP-8 and to some extent diesel was observed. The relative amounts of olefins and n-paraffins decreased with the products distribution shifting more towards the production of isomers.

Key words:: MixAlco process; response surface method; pyrolysis; sludge; syngas composition; efficiency; pressure swing adsorption; cycle bed productivity; % recovery, % purity; Fischer-Tropsch synthesis; JP-8; gasoline; diesel; selectivity; Co-SiO_2/Mo-Pd-Pt-HZSM-5 catalyst

DEDICATION

This Dissertation is dedicated to the following:

my wife Mirabel Teiseh

my dad Amadou Teiseh

my mother Aramatou Teiseh

ACKNOWLEDGEMENTS

I would like to thank my committee chair and major advisor Dr. S. Capareda for giving me the support and contributions that led to the realization of the work. My appreciation also goes to the other committee members viz: Dr. S. Fernando, Dr. J. Holste and Dr. R. Karthikeyan for their inputs that helped improve the results of my work.

NOMENCLATURE

Meanings of symbols and their units

MC=moisture content (wt %)

VCM=volatile combustible matter (wt %)

FC=fixed carbon (wt %)

Hv_g=heating value of syngas (MJ/kg)

BO=bio-oil

M_f=mass of sludge pyrolyzed (kg)

W_s=auger shafting work (J)

P.dV=work done on system (J)

Q=thermal energy supplied (J)

ΣE_g=total energy of syngas (J)

E_b=energy of bio-oil (J)

E_c=energy of char (J)

ΣM_g=total energy of syngas (J)

M_b=mass of bio-oil (kg)

M_c=mass of char (kg)

V_t=total volume of syngas (L)

C_g=concentration of syngas (v %)

P=P*=1 atm

t_{br}=breakthrough time (minutes)

ρ=density of H_2 at standard conditions (g/L)

Ø= mol fraction of H_2 in feed (mol %)

Q= feed flow at standard conditions (SLPM)

p= hydrogen purity (%)

ζ=dimensionless parameter relating axial distance bed length and pressure drop

P_{atm} = atmospheric pressure (atm)

D_k = Knudsen diffusivity (m^2/s)

D_m = molecular diffusivity (m^2/s)

T=temperature (^oC)

M=molecular weight (g)

r=radial coordinate in microparticle

D= Poiseuille diffusivity (m^2/s)

μ= viscosity ($gcm^{-1}s^{-1}$)

R= universal gas constant, 0.08205, Latm/K/mol

$\dot{n}_{\text{ideal gas}}$ = molar feed rate of ideal gas $\left(\frac{\text{mol}}{\text{standard liter}}\right)$

$\dot{Q}_{\text{ideal gas}}$ = volumetric feed rate of ideal gas(standard lpm)

$p_{\text{ideal gas}}$=feed partial pressure of ideal syngas (atm)

A_i = GCMS peak area of hydrocarbon i in the effluent stream

n=number of liquid hydrocarbons produced per experimental run

W_{cat}=catalyst weight (g)

GHSV= gas hourly space velocity ($minute^{-1}$)

$Feed_{\text{ideal gas}}$ = feed rate of ideal synthesis gas (standard lpm)

TABLE OF CONTENTS

Page

Page

LIST OF FIGURES

Page

LIST OF TABLES

CHAPTER I
INTRODUCTION

1.1 Background

In order to produce gasoline, JP8 and diesel fuel, the MixAlco process developed by Professor Mark Holtzapple of the Department of Chemical Engineering of Texas A & M University in College Station ferments (using a mixed culture of acid-producing micro-organisms) wastes from paper and pulp and mixed food residues to produce carboxylate salts. The salts are thermally converted to ketones which are then hydrogenated into a mixture of alcohols. Then a ZSM-5 catalyst converts the alcohols to hydrocarbons [1].

The problem is that, for every 40 tons per hour (on a dry basis) fed into the MixAlco process, about 8 tons per hour (on a dry basis) is produced as undigested material (personal communication, Dr. M. Holtzapple). The undigested material is then wasted as effluent sludge. The enormity of the sludge that will be produced annually in a scaled up plant becomes obvious. The associated waste management and the environmental and health externalities will be a burden for the proponents of the process. A schematic of the MixAlco process is shown in Figure 1.1.

This dissertation follows the style of Biomass & Bioenergy Journal.

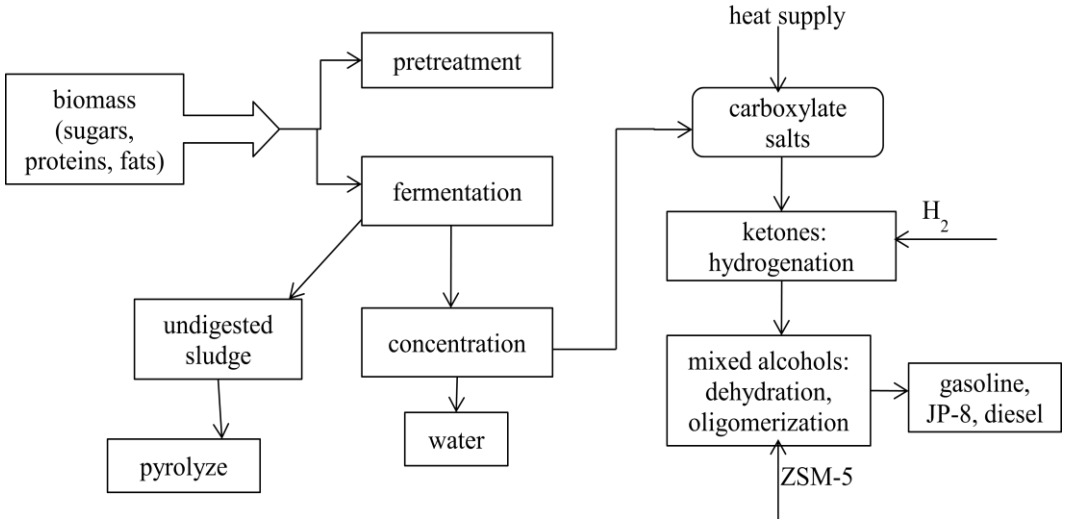

Figure 1.1 The MixAlco process for the conversion of wastes to liquid fuels

Although iron based Fischer-Tropsch synthesis catalyst has been largely employed in biomass-to-liquid synthesis process, iron catalysts are prone to deactivation. Also use of iron leads to a reduction in the productivity of higher hydrocarbons. The use of iron instead of cobalt is validated by the fact that the hydrogen production potential of biomass feedstock is low compared to steam reforming of methane which is usually accompanied by the WGS reaction.

Since iron catalyst catalyzes the WGS reaction, this reaction is usually employed as part of the overall conversion scheme to increase the H_2:CO ratio to a level amenable to the production of heavier hydrocarbons. The problem is that relying on internal H_2:CO ratio adjustment constrains the ability to operate at a desired target syngas composition necessary for optimum cobalt catalyst performance. Secondly compared to cobalt, iron catalyst has a lower productivity to higher hydrocarbons in the jetfuels and diesel boiling range [29,33].

The pyrolysis of the MixAlco process sludge and other biomass feedstocks will generate syngas (H_2 and CO) together with methane. External modification of the final syngas composition for use in the FTS catalyst may involve the steam reforming of the

CH_4 (after separation using PSA) to achieve the feed gas in appropriate composition for cobalt catalyst. Cobalt catalyst performs optimally at a H_2: CO ratio of 1.7-2.0 in the production of liquid fuels.

In this work we show how the syngas from the pyrolysis of the MixAlco process sludge in the approximate H_2:CO ratio of 1.3 (~45 v% H_2 and 35 v% CO) can have its H_2:CO ratio increased to 1.9. The proposed external modification of the composition of the syngas is shown in Figure 1.2 for 1 ton of sludge pyrolysed. This is achievable through the steam reforming of a third CH_4 product produced in a concentration of up 20.3 v%. The gasoline, jetfuel and diesel generated from this process will increase the overall yield and capacity of the MixAlco process.

Higher temperature pyrolyis (700 to 950 ^oC) in particular is known to increase the yield of syngas, although bio-oil and char yields both decrease under those conditions [7]. A moving fixed bed pyrolyzer will at different sludge feeding rates pyrolyze the sludge at temperatures in the range of 630-770 ^oC to optimize the production of synthesis gas.

Our main goal is to show how liquid transportation fuels (typically hydrocarbons in the JP-8 carbon number range) can be produced from the sludge produced by the MixAlco process. This is possible by integrating pyrolysis, pressure swing adsorption and Fischer-Tropsch synthesis processes.

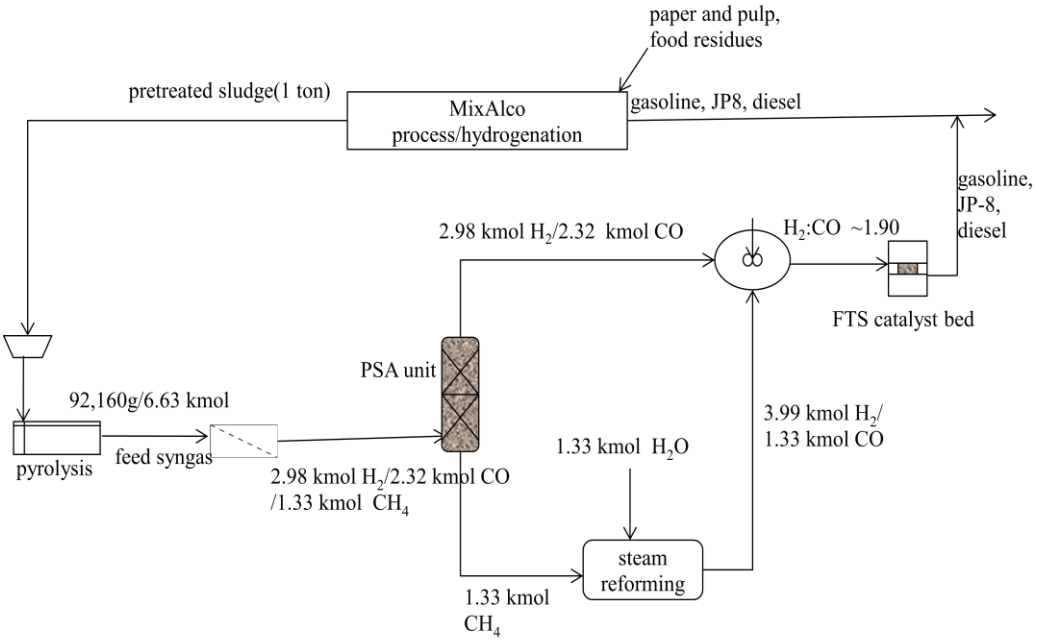

Figure 1.2 Adjustment of H_2: CO ratio by steam reforming of CH_4 produced by sludge pyrolysis

The syngas production potential of some biomass feedstocks can be significantly high. In a 300 W microwave pyrolyzer for example the pyrolysis of rice straw gave volumetric syngas yields of 55 % H_2/17 % CO_2/ 13 % CO/10 % CH_4 [16]. Using a conventional fixed bed pyrolysis at 650 ^oC the total syngas volumetric yields of wastewood, cardboard and textile feedstocks were respectively 41.3 %, 42.3 % and 45.8 % in a separate study [9].

The hydrogen separated from the syngas by pressure swing adsorption (PSA) can be used in the hydrogenation of ketones in the MixAlco process to produce liquid transportation fuels. Another possibility will be to separate the methane from the syngas (by PSA) so that the key components, H_2 and CO can be catalytically converted to higher hydrocarbons using an enhanced Fischer-Tropsch synthesis process. Hence the three main objectives to be attained are the following:

1. Maximize the production of syngas (H_2 and CO) and/ or CH_4 from the sludge derived from the MixAlco process.

The hypothesis is that, if temperature and biomass feeding rate are factors that affect the composition of syngas generated from the process of sludge pyrolysis, then there should be a combination of temperature and/or feeding rates for which the concentrations (v%) of hydrogen, carbon monoxide and methane are potentially all or individually maximum.

2. Determine ½ cycle bed recovery that is based on an optimum cycle bed productivity from a critical amount of adsorbent with savings on adsorbents used in the separation of hydrogen from low concentration synthesis gas streams.

The second hypothesis is that *there is a given amount of adsorbent that gives maximum cycle productivity (ie cycle mass of hydrogen obtained per unit mass of adsorbent used).* That amount of adsorbent (if it exists) applied to low concentration sygas streams will lead to the use of a two-bed PSA system for efficient product recovery versus multiple-bed systems.

3. Design and test a novel Fischer-Tropsch (Co-silica/Mo-Pd-Pt-HZSM-5) hybrid catalyst that produces even longer chain hydrocarbons(in the JP-8 and diesel carbon number range) from syngas compared to Co-silica.

The third hypothesis is that *a hybrid Co-SiO_2/Mo-Pd-Pt-HZSM-5 catalyst can increase the selectivity of hydrocarbons in the JP-8 and diesel carbon number range versus normal Co-SiO_2 at lower temperatures and pressures in a fixed bed reactor mode of operation.*

One of the primary benefits of the conversion of the sludge to useful products is that the minimum selling price of the fuels produced from the original biomass feedstock will be reduced to less than their estimated US $1.24/gallon [1]. This is justified because this price tag was arrived at assuming that the market price of the externally supplied hydrogen will be US $1/kg [1]. The fuels production capacity of the plant will also

increase. Given that the effluent sludge constitutes waste that might have to be dealt with otherwise, waste management costs are also saved. Other benefits include environmental cost savings and derived carbon credits. Generally speaking, this makes the MixAlco process competitive, even without government subsidies.

1.2 Review of Related Literature

1.2.1 Biomass pyrolysis into syngas, bio-oil and char

Hydrogen, carbon monoxide and methane constitute components of synthesis gas although ideally pure syngas contains only hydrogen and carbon monoxide in specific proportions for liquid fuels production, especially via the Fischer-Tropsch synthesis process (FTS) [2-4]. Syngas is a building block for a variety of fuels and chemicals. Hence the syngas(from biomass) platform for the production of liquid transportation fuels represents a re-articulation of the lignocellulose-to-liquid fuels pathway [5].

As a renewable energy source, biomass is derived from carbon-based materials and its environmental benefit is carried in its being carbon neutral – the carbon dioxide emitted during its combustion equals the amount consumed during carbon fixation in photosynthesis [7-8]. Pyrolysis process is more energy efficient and is energy neutral especially for commercial and industrial feedstocks [10]. Perhaps it is in part for this reason that in the UK, Renewable Energy Obligation Certificates (ROCs) are issued as an incentive for the setup and operation of pyrolysis units [9].

During pyrolysis, organic matter is depolymerized/decomposed in the absence of oxygen to produce syngas, liquid (bio-oil) and char. Because of a broader product distribution, the process (especially fixed bed pyrolysis) is sometimes preferred over gasification because product gas dilution by the fluidizing gas is not an issue. Pyrolysis involves dehydration and decarboxylation as primary reactions at low temperatures and secondary cracking reactions of phenols and carboxylic acids at higher temperatures. The bio-oil can be catalytically converted into liquid fuels, upgraded and combusted, providing heat to process boilers. The char can be used to make activated carbon applied

to soils to enhance productivity, or used to make carbon electrodes [9-11]. The syngas like bio-oil can be combusted in combustion units such as boilers and the thermal energy recycled to sustain the process or converted into liquid fuels in an add-on catalytic process [10, 12-14].

Fast or slow pyrolysis can be defined based on the biomass temperature heating rate or the residence time of the biomass in the reactor. Operating under isothermal conditions, the defining parameter becomes the residence time or biomass feeding rate. For a given residence time (feeding rate) the heating rate becomes the defining parameter. Reactor configurations include auger driven, ablative, vacuum or fluidized beds.

A number of studies have been done on resource recovery and environmental preservation or management through the pyrolysis of agricultural wastes, municipal solid wastes (MSW) or sewage sludge. Various feedstocks pyrolyzed under different conditions of temperature, pressure, feeding rates and heating rates result in products in different amounts in fluidized beds, auger driven, ablative or vacuum reactors [49].

For example, the fast pyrolysis of Japanese larch produced higher bio-oil at lower temperatures with a maximum obtained at 450 ^{o}C. As the temperature increased, syngas production increased, while char production decreased. This is attributed to the promotion of secondary cracking reactions at higher temperatures which convert the bio-oil and char to gaseous products. In a fluidized bed system, enhanced bio-oil recovery is observed because of improved mass and energy transfer efficiencies. In particular more bio-oil is recovered when the product gas is used as the fluidizing medium, since they also take part in gas phase secondary reactions, producing organic phase chemical species [15]. An increase in the residence time (lower feed rate) leads to a reduction in the bio-oil yield and an increase in the syngas yield [49-50].

Microwave oven pyrolyzers have also been used for the pyrolysis of biomass. Huang et al (2008) pyrolyzed rice straw in a microwave oven significantly reducing its fixed carbon content and producing up to 55 v% of hydrogen in the product gas stream.

The amount of harmful poly-aromatic hydrocarbons produced in the liquid phase was also reduced. Use of microwave technology is again based on higher energy efficiency since energy is converted from electromagnetic to thermal energy directly and does not have to be transferred in the dielectic (microwave adsorbing materials) [16].

Little attention has been devoted to the thermo-chemical conversion of biomass sludge to useful resources such as syngas (the hydrocarbons building blocks in the gas – to- liquid technology) eventhough the United States produced up to 6.9 million tons of dried sludge in 1998 and was estimated to reach 8.2 million tons in 2010. China also was expected by estimates to generate an identical 8.0 million tons (dry basis) in 2010 [17]. There is therefore little or no literature information with regards to the maximization of syngas concentrations from sludge using a moving fixed bed auger driven pyrolyzer with consideration given to mass and energy balances for process efficiency purposes. The moving fixed bed auger system has the advantage that we don't have to worry about the dilutions of product synthesis gas by the fluidizing fluid, usually nitrogen. This makes the separation of hydrogen or methane [for the case where conversion of H_2 and CO to liquid fuels is the preferred route] relatively straightforward from a technical and system complexity standpoint. The optimized hydrogen in the syngas can be separated by pressure swing adsorption for use in the MixAlco process.

1.2.2 Hydrogen separation by pressure swing adsorption

1.2.2.1 Merit of the technology and principles

Low to medium scale plants are increasingly embracing pressure swing adsorption (PSA) as the separation technology of choice. This is evident by the number of PSA patents filed per year. There has been an increasing acceptance for its use in the recovery of raffinate product from traditionally low-concentration feed streams such as in the recovery of methane from anaerobic fermentation products of digesters in wastewater treatment plants or from landfill biogas [17-18]. In PSA systems the impurity (more strongly adsorbed adsorbate) is retained on the adsorbent, while releasing a

product stream enriched in the less strongly adsorbed adsorbate at higher pressures. The more strongly adsorbed gases are released when the pressure swings to a lower value.

PSA has traditionally seen applications in cases where H_2/CO mole ratios in the synthesis gas are greater than 2 (as for syngas derived from the steam reforming of methane). There is the need to adjust the H_2/CO ratio to a value suitable for optimum catalytic performance in adjoining gas-to-liquid conversion processes. Such higher H_2/CO mole ratios are produced in industrial syngas production processes using natural gas rather than biomass as the feedstock [6]. With a higher feed CH_4 concentration, the flexibility of the technology also allows the adjustment of the syngas compositions either by way of complete removal of methane (usually not desired in feeds) or otherwise for biomass-to-liquid conversions processes such as FTS. Again, PSA technology is more competitive for low to medium capacity gas production plants.

1.2.2.2 PSA systems design

The design of a PSA packed adsorption separation column begins with selection of appropriate adsorbent whose interaction with the adsorbates creates two broad separation modes – sorption equilibrium or kinetic rate based separations [24]. In equilibrium based separation (studied using the linear driving force model), mass transfer of one adsorbate to the adsorbent surface is greater than for its competing counterparts. The adsorbate with less mass transfer to the adsorbent leaves as the separated product. For kinetically based separation (studied using diffusivity model), the selective sieving of smaller molecules through the pore sizes leads to a greater bulk gas phase mass transfer of the smaller molecule as the enriched gas phase product.

Equilibrium or kinetically based isotherms for the separation of various gases using activated carbon, zeolites, or carbon molecular sieves can be generated or are available in the literature. Using Langmuir, Freundlich, Langmuir-Freundlich, ideal adsorbed solution theory or vacancy solution models, the sorption isotherm of pure or multiple component mixtures can be obtained and then used with the Brunauer's

classification to reckon an isotherm as favorable (type I) or unfavorable (types II, II, IV). This determines the selection of blowdown, purge(in terms of selection of purge to feed ratio) or desorption steps (co- or counter-current to feed, or at subatmospheric or atmospheric conditions) in overall PSA cycle [24]. Model parameters calculated from such isotherms can also be used in overall process models used in process performance simulations [20-22]. Breakthrough curves are generally used to study the dynamics of the wavefront or concentration profile of the impurity that characterizes the mass transfer zone separating the saturated zone behind it from the fresh adsorbent zone rich in the product in front [22-23].

1.2.2.3 Literature findings

The key output parameters used to study PSA systems are % purity, % recovery, and productivity. Each of these parameters can be changed by changing other input design parameters such as adsorbent particle size, cycle time, feed pressure, bed configuration, pressurization, purge with product or external hydrogen and increasing the number of beds per cycle. For example, an increase in the number of beds has little or no impact on the % purity but could dramatically increase % recovery by over 50 %, while an increase in the total cycle time decreases the purity, and increases the recovery. Yang et al (2009) found that an increase in % recovery with linear velocity of feed flow only occurred to a certain extent after which recovery dropped due to a broadening of adsorption wave front in the bed [24-26].

The experimental studies by Shivaji et al (2011) showed that an adsorbent particle size of 0.35 mm, a total cycle time of 3-5 s and a feed pressure of 2.9-4.0 atm produced an O_2 recovery of ~25-35 % for a percent purity of ~90 % O_2 in the product stream in a novel PSA unit for medical oxygen concentrator [27]. Separation of one component from a ternary mixture where 2 gases have almost identical separation factors on one adsorbent is achieved by splitting the separation process between two or more layered adsorbents. Layered bed configurations are also used in ternary gas

mixtures when one of the impurity species has a significantly favorable sorption isotherm with respect to the first adsorbent. This permits the separation of the product from the remaining species on a second top bed where the adsorption of the less desired species is much stronger. Hydrogen has been separated in a 4-bed PSA system to a 99.999 % purity and a recovery up to 66.00 % using a double adsorbent of activated carbon and molecular sieve 5A with feed gas having the composition, 72.2 % H_2/21.6 % CO_2/ 2.03 % CO/ 4.17 % CH_4 and derived from the SRM process. It was found that increasing the time in the adsorption step from 40 to 50 seconds caused the recovery to improve from 58 to 66 %, although the purity remained unaffected [28].

1.2.2.4 Maximizing PSA H_2 recovery from low H_2 concentration syngas

In order to recover hydrogen from a low concentration pyrolysis gas stream (for use in the hydrogenation of ketones in the MixAlco process) with minimal complexity and costs, yet achieving efficient product cycle recovery, we propose to use a layered bed configuration of activated carbon and molecular sieve 5Å. By doing breakthrough curve and cycle mass balance studies for different amounts of adsorbents, a specific amount of adsorbent that gives optimum cycle bed productivity will be determined.

It is hoped that using this amount of adsorbent in PSA systems will reduce the number of beds and complexity hence saving costs and optimizing product recovery especially for a low hydrogen pyrolysis syngas. One alternative route is to select an adsorbent that will selectively adsorb CH_4 enriching a product of H_2 and CO for use in an enhanced Co-SiO_2/Mo-Pd-Pt-HZSM-5 hybrid Fischer-Tropsch synthesis process to increase selectivity in the JP8 and diesel range. This when fed into the MixAlco process will increase its fuels production capacity.

1.2.3 Fischer-Tropsch synthesis process for syngas conversion to liquid fuels

1.2.3.1 History and products distribution

The Fischer-Tropsch synthesis (FTS) process, named after two German pioneers Han Fischer and Franz Tropsch converts syngas to hydrocarbons over transition metal catalysts supported on basic metal oxide supports producing diesel and heavy waxes [29]. Fundamentally, FTS process involves the hydrogenation of CO followed by polymerization of monomers over transition metal active sites. The product distribution is statistical and follows the Anderson-Schulz-Flory probability model. Hence there is only a 48 % chance of producing a hydrocarbon within the desired gasoline range (C_4 to C_{12}). This means that as the probability for chain growth increases, the selectivity of higher hydrocarbons and waxes increases dramatically [30].

1.2.3.2 Catalyst design

The design of heterogeneous catalytic systems involves some unit operations such as impregnation (typically achieved by pH controlled ion-exchange between the support surface and precursor solution), precipitation, deposition-precipitation. Other new techniques include sol-gel, eggshelling, colloidal, microemulsion, solvated metal atoms and dispersion. Intended to transfer the precursor to the support surface with optimum dispersion, and hence maximum active surface area, each of these methods will be able to maximize key design and assessment metrics such as specific conversion (or specific activity), selectivity, stability and revivification (or regenerability). Their selection and use depends on intended catalyst loading, interaction between catalyst nanoparticles and support and whether a homogeneous or inhomogeneous dispersion will result.

All these directly affect activity or deactivation and overall performance of the catalyst [31-32]. Drying allows improved dispersion of the precursor followed by

calcining to convert the precursor to its oxide form. The oxide is then reduced to the pure metal active form in a hydrogen reduction step. Post preparation parameters such as hydrodynamics, retention time, reactor configuration and alignment, amount of catalyst, and thermodynamics affect performance of the catalyst [33].

1.2.3.3 Fischer-Tropsch synthesis catalysts in biomass-to-liquid technology

Cobalt and iron are generally used although iron is used mainly for low hydrogen syngas sources such as biomass and coal. It is however more temperature flexible while cobalt being more temperature sensitive is more active at low temperatures with an enhanced production of higher hydrocarbons. For cobalt catalysts in general, a specific feed composition results in ideal performance with selectivity of higher hydrocarbons achieved with increase in pressure although addition of modifiers achieves the same effect with a reduction in methane selectivity [29,33].

1.2.3.4 Tuning the product selectivity

To promote secondary reactions or reformation reactions that lead to the production of longer chain alkanes and alkenes (with increased energy output), and isomers and aromatic hydrocarbons (with a higher octane rating), new interests are being developed in coupling FTS catalyst with zeolites in a hybrid system that may be either single-stage (with thermodynamic constraints) or two-stage (with no thermodynamic constraints). Depending on the catalyst of choice, in-situ deactivation resulting from the migration of OH^- to the acid zeolite might dictate catalyst bed as either physical admixture or dual layer configuration. Such setups create a bi-functional catalytic system with a metal activity on the FTS catalyst and an acid activity on the zeolite catalyst [13,34]. Typical secondary reforming reactions on zeolite include: an acid functionality such as long-chain hydrocarbons cracking and transition metal functionality such as isomerization, oligomerization and/or polymerization of shorter chain hydrocarbons and

aromatization (at high temperatures and pressures) of products from the FTS process. This means that a ZSM-5 zeolite with a low Si/Al ratio can have an acid-metal functionality when those metals are in low concentrations.

The rationale for using Fe instead of Co in biomass to liquid processes is to exploit the ability of the former in catalyzing the water-gas-shift reaction to enhance the H_2/CO ratio to an acceptable value to increase the yield to higher hydrocarbons. The pyrolysis of paper- and pulp-derived sludge from the MixAlco process can produce a relatively high amount of CH_4 and synthesis gas (compared to coal). SRM and modification of the syngas composition can be used for the production of liquid transportation fuels (with higher selectivity of higher hydrocarbons) using cobalt instead of iron. This by-passes the water-gas shift reaction internal modification process that relies on proper functioning of the iron catalyst among other factors.

Hence the main objective of this part of the work will be to produce liquid transportation fuels in the gasoline (C_4 to C_{12}) and jetfuel or JP-8 (C_{10} to C_{17}) using a hybrid Co-SiO_2/Mo-Pd-Pt/HZSM-5 tri-functional metal-metal-acid environment versus the bi-functional environments currently proposed in literature. This novel hybrid FTS catalyst will extend the capability of the conventional FTS cobalt catalyst to the production of a fuel with more JP8 and diesel that can be fed into the transportation fuel product stream of the MixAlco process. Throughout this work future references to selectivities of gasoline, JP-8 and diesel will mean selectivities of hydrocarbons with carbon numbers in the ranges C_4-C_{12}, C_{10}-C_{17} and C_{15}-C_{25} respectively.

CHAPTER II
PYROLYSIS OF MIXALCO PROCESS SLUDGE TO SYNTHESIS GAS

2.1 Experimental

2.1.1 Experimental setup

The schematic of the process is shown in Figure 2.1. A moving bed auger pyrolyzer having a hopper with the dimensions 2 ft by 2 ft by 4.25 ft was used for the experiments.

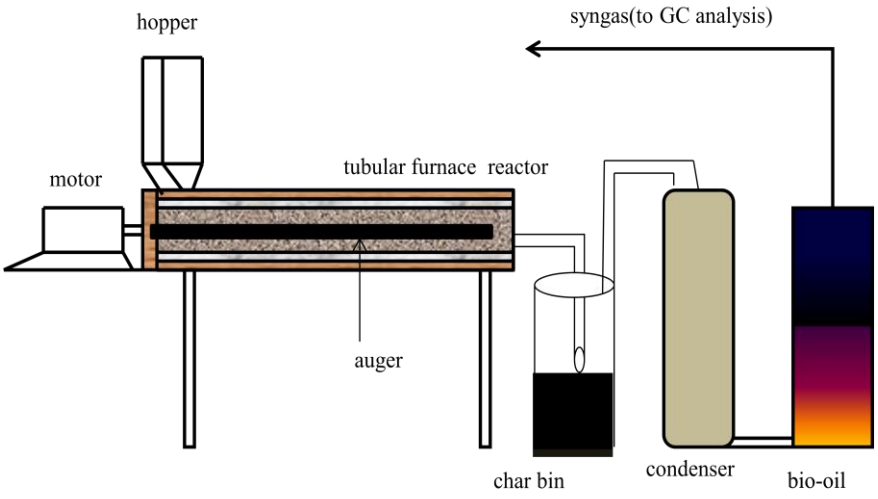

Figure 2.1 A schematic representation of an auger (moving fixed bed) pyrolyzer for the conversion of sludge to syngas

The pyrolysis reaction occurred in the heated middle zone of a tubular furnace heated electrically by a Linberg/Blue M heater supplied by Thermoelectron Corporation/Centigrate Service Inc (Ashville, North Carolina). The tube furnace, also a

Linberg/Blue M type was also supplied by Thermoelectron Corporation/Centigrade Service In.c (Ashville, North Carolina). The furnace chamber contained a 0.3 ft nominal diameter cylindrical tube containing an auger. The cylindrical tube was a conduit for the feedstock. The sludge was initially fed into a hopper, which was connected to the heated zone of the reactor. A 2.5 amps Honeywell electric motor (Rockford, Illinois) provided rotational and translational motion of the auger, which in turn moved the ground sludge into the reactor.

2.1.2 Calibration

The biomass feeding rates were varied from a calibration curve relating the number of auger RPMs to the biomass feed rates. The hopper was fed with the pretreated sludge at room temperature and pressure and the time taken for a given amount of the feedstock to move from the hopper to the char collection bin was recorded for a given RPM. The biomass feed rate was then determined by dividing this amount collected by the recorded time. Runs for each RPM were performed in duplicate.

Auger RPMs of 2.6, 3.0 and 3.4 corresponded to 290, 330 and 374 g/minute of biomass fed. By setting the auger to a given RPM, a specific value for the sludge feed rate could be predetermined. Since preliminary experiments showed that hydrogen, carbon monoxide and methane will be the gases produced, the GC was previously calibrated for these gases using a gas standard with the composition, 20 v% CH_4/20 v% H_2/ 20 v% CO with the balance being nitrogen. The established calibration curve is diagrammed in Figure 2.2.

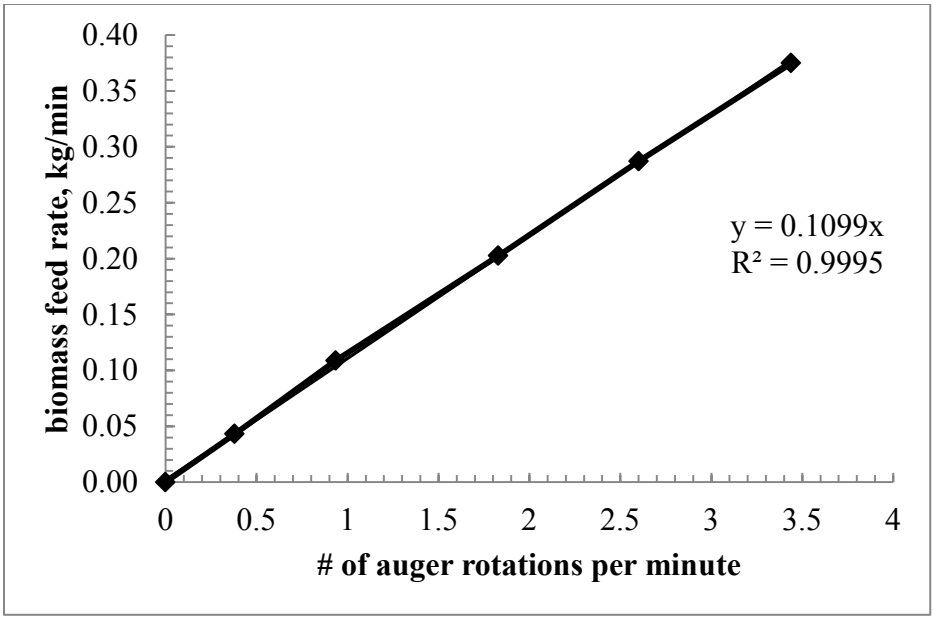

Figure 2.2 Biomass feeding rate versus auger rotations per minutes

2.1.3 Sludge pretreatment and analysis

The sludge was dewatered by sun-drying until almost all of its moisture was removed ("bone dry"). A bone dry sludge was one whose moisture content was less than 10 wt %. The dewatered sludge was then crushed to powder form to facilitate its movement into the heated zone of the furnace. Proximate analysis included the determination of volatile combustible matter (ASTM D 3175-07), moisture content (ASTM E 871-82 reapproved in 2006), ash content (ASTM D1102-84 reapproved in 2007) and fixed carbon. To determine the moisture content, pretreated sludge was dried constantly until its moisture content was <10 wt %. The dry feed stock was volatilized at 950 ^{o}C in a furnace for 15 minutes and the volatile combustible matter (VCM) calculated as the percentage loss in weight. The ash content was determined using the residue from the VCM determination experiment and was further heated at 550 ^{o}C for 4 hours and the weight of the residue expressed as a percentage of the weight of the dry feed stock, after

the loss of the fixed carbon. The fixed carbon content was determined by arithmetic difference.

Minerals analysis was done by Huffman Laboratories (Golden, Colorado). Before analysis, the samples were centrifuged and the free aqueous layer (containing dissolved organics) was removed. All the results were reported from the remaining organic fraction. Ash was determined by stage ashing in air to a final temperature of 750 ^{o}C and holding at that temperature for 8 hours. The heating values of the feedstock, char and bio-oil were determined using a Parr 6200 bomb calorimeter supplied by Parr Instruments Company (Moline, Illinois). The heating values of the syngas used were values reported in Perry et al (1984) [52] and are shown in Table 2.1.

2.1.4 Pyrolysis experiments

Between 2,240 and 3,400 g of the dry feed was fed into the hopper of the pyrolyzer per run. Runs were carried out isothermally at 630, 680, 730, 750 and 770 ^{o}C and at atmospheric pressure conditions. Three sludge feeding rates of 290, 330 and 374 g/minute were studied in different combinations with the temperature. After feeding and tightening the hopper, the furnace was then heated to the preset temperature. The furnace temperatures were measured by installed J-K type thermocouples. The entire system was purged for 25 minutes with industrial grade nitrogen (98.9 % purity) supplied at a flow rate 250 ml/minute (to create an oxygen free environment) at the end of which sludge was delivered into the reactor by the auger system. To enable the condensation of condensable gases into bio-oil following pyrolysis, the condensable and uncondensable gas mixture was passed through a 0.5 inch internal diameter stainless steel pipe immersed in ice-frozen water. A line of the uncondensed syngas stream was passed through an online Horiba digital gas analyzer, supplied by Horiba Instruments Inc. (Ann Arbor, Michigan).

The first product of the process (char) was collected into a char collection bin. The condensable and non-condensable products went through a condenser where bio-oil

was recovered from the condensable gases. The non-condensable gases then left as the desired synthesis gas. The experiments were performed at atmospheric pressure conditions in triplicates for each combination of temperature and biomass feeding rate. Total experimental run time was between 20-25 minutes.

2.2 Experimental Design

A direct approach used for a process optimization is the response surface method (in a central composite design) frequently employed in statistical studies for the optimization/minimization of a given parameter [51]. The technique was employed here to determine the set of temperature and biomass feeding rates needed for the optimum production of some or all of hydrogen, methane and carbon monoxide. For our range of temperature and biomass feeding rates, preliminary results showed a response surface center point (temperature, feeding rate) of (750 ^{o}C, 329 g/min). Above this combination, syngas concentration seemed to increase for each component and decreased below it. Actual experimental runs were therefore initially done for a range of temperature between 730 to 770 ^{o}C for the three biomass feeding rates of 290, 330 and 374 g/min.

The results were analyzed to see the influence of each parameter. Since fractional volumetric gas production seemed to peak at this temperature range, for all feeding rates, a meaningful gas production trend was established by extending to lower temperatures of 630 ^{o}C and 680 ^{o}C, at a feeding rate of 329 g/min. This gave a 1/2 factorial design for a total of 21 experiments from a possible total of 45. The stated hypothesis (H) was that:

H: *If temperature and biomass feeding rate are factors that affect the composition of syngas generated from the process of sludge pyrolysis, then there should be a range temperature and/or feeding rates for which the concentrations of either hydrogen, carbon monoxide or methane and some other possible combinations thereof are maximum.*

2.3 Mass and Energy Balances

The flow of material (energy and mass) in and out of it is shown in Figure 2.3. An energy and mass balance on this control volume was performed. Gravimetric measurements of masses in and out of the pyrolyzer and the determination of energy contents of feed and products from their heating values were used to calculate mass recovery and energy efficiencies. The heat contents of the products and feed sludge were calculated as shown in Eqs.2.1-2.2.

The ratio of the sum of the energies of the products to the electrical energy needed or of the sum of the mass of the feed to the combined mass of the products quantified energy and mass recovery efficiencies as shown in Equations 2.3-2.4. The ratio of the energy of the products to the electrical energy needed to pyrolyze the feedstock was used to establish the energy neutrality of the process. A ratio of at least 100 % meant energy neutrality.

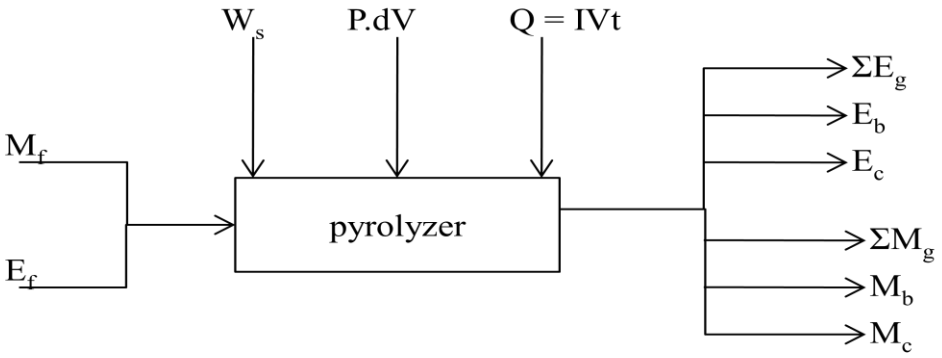

Figure 2.3 Material flow in and out of pyrolyzer (for energy and mass balances)

Energy of syngas $=\Sigma E_g=\Sigma \frac{P^* \times M \times V_t}{RT} \times C_g \times Hv_g$……..…..……..…2.1

Non-sygas product energy $= mass \times Hv_g$ ……..…..……...……2.2

$$\text{Energy efficiency (\%)} = \frac{\Sigma \text{m.Hv}_{\text{product}}}{\text{m.Hv}_{\text{dry sludge}}} \times 100 \text{……..……2.3}$$

$$\text{Mass efficiency (\%)} = \frac{\Sigma \text{m}_{\text{product}}}{\text{m}_{\text{dry sludge}}} \times 100 \text{……..……..……2.4}$$

2.4 Data Collection and Analysis

The amount of sludge pyrolyzed was the difference between the amount fed into the hopper and the amount left unpyrolyzed. The amounts of char and bio-oil produced were determined gravimetrically. The syngas produced was directed into gas balloons as it exited the effluent line. Since these balloons were spherical, their volumes were easily calculated. The total volume of the synthesis gas produced together with its concentration (v%) were used to determine the mass of each constituent by first determining its density at room temperature and pressure using the ideal gas law. These masses were then used in mass balances to determine the mass recovery. The products of the masses of the feedstock or the products and their respective heating values were used in energy balance calculations.

During each run, a triplicate sampling of the syngas was performed although each set of pyrolysis condition was examined also in triplicate. Peak readings on the Horiba output display gave indications of the maximum compositions of the synthesis gas that would be obtained under steady state constant pyrolysis of the feedstock for all conditions of temperature and feeding rates. Samples were collected in 1.0 L Tedlar bags supplied by SKC Inc (Houston, Texas) when readings close to this optimum composition were observed and analyzed using an 8610C SRI GC (Torrance, California) equipped with a TCD and an HID detector. The GC column temperature program maintained an initial column temperature of 60 ^{o}C for 5.0 minutes which was ramped to 220 ^{o}C at a

ramp rate of 20 ^{o}C/minute. It was maintained at this temperature for 30 minutes before cooling to 60 ^{o}C in a column reconditioning subprogram.

The percent composition results from the GC were analyzed using the Design Expert® software to arrive at a quadratic response surface model for each gas species. The spread of the data was reported in terms of standard deviations by Design Expert® software. The results were statistically analyzed using the analysis of variance (anova) at the 95 % confidence level.

2.5 Results and Discussion

2.5.1 Sludge and products characterization

The proximate and mineral analyses and the heating values of the pretreated sludge and products are shown in Table 2.1. The volatile combustible matter (VCM) content of the feedstock was the highest. This is typical for most sludge biomass especially sludge from industrial sources. The VCM gets converted into gaseous products at higher pyrolysis temperatures [9,10,17-18].

The biomass structure also contained Ca, Fe and Mg known for their catalytic activities in converting oxygenates into hydrocarbons and hydrogen at higher temperatures. The low S content of the biomass minimizes the production of sulfur compounds or gases in the products stream. This means that the catalytic upgrade of products from the pyrolysis of the sludge has a low chance of being plagued with sulfur catalyst poisoning [33,44]. The enriched hydrocarbons content of the bio-oil explains why its heating value is highest. The conversion of the fixed carbon of the sludge into other products during pyrolysis leads to a fall in the heating value of the char produced [7].

Table 2.1 Proximate and mineral analyses and heating values

proximate analysis (wt %)								
			MC	VCM	FC	Ash		
			7.2±1.6	66±2.1	3.1±3.2	23.7±1.8		
mineral analysis (wt %)								
S	Al	Ca	Fe	Mg	P	K	Si	Na
0.7	0.3	9.2	0.2	0.2	0.7	0.1	0.5	0.1
heating value (MJ/kg)								
		sludge	char	bio-oil	H_2	CH_4	CO	
		13.71±2	10.7±2.9	25.6±3.6	120	49.8	10.2	

2.5.2 Optimum synthesis gas production and the anova model

The statistical model for the optimization of the concentrations of hydrogen, methane and carbon monoxide was significant with a p-value <<0.05. Temperature was also important as a main effect variable determining the composition of syngas with a p-value (α)<<0.05. The interaction between temperature and feeding rates was not significant (p-value >0.05). The feeding rate also turned out not to be significant in influencing syngas production (p-value >0.05) (Table 2.2). This could be explained partly by the fact that the range of feeding rates studied was narrow. It is possible that temperatures in the range 630 ^{o}C to 770 ^{o}C were high enough to de-polymerize the sludge biomass into products making feed rate not really significant. That might explain why statistically there was no significant interaction between the two parameters. In

particular, temperature has been reported to be the dominant factor influencing product yield in pyrolysis [16].

A normality test revealed that the error distribution of the data for all three gases was approximately normal with the data fitting a straight line as shown in the normal plot of the residuals in Figure 2.4 for hydrogen concentrations only. The significance or non-significance of the models and parameters of temperature (T) and sludge feed rate (F) are shown in Table 2.2 with the generated best-fit regression models for hydrogen, carbon monoxide and methane concentrations(v%) shown in Eqs.2.5-2.7.

Table 2.2 Anova for response surface quadratic model
a) Response 1: Hydrogen concentrations statistical analysis

source	sum of squares	deg of freedom	mean square	F value	p-value, prob >F	significance
model	1404	5	280.9	24.9	<0.0001	significant
T: temperature	765.9	1	765.9	67.9	<0.0001	significant
F: feed rate	3.9	1	3.9	0.35	0.56	not significant
TF	5.6	1	5.6	0.5	0.49	
T^2	47.5	1	47.5	4.2	0.05	
F^2	0.35	1	0.35	0.031	0.86	

Table 2.2 continued

b) Response 2: Carbon monoxide concentrations statistical analysis

source	sum of squares	deg of freedom	mean square	F value	p-value, prob >F	significance
model	118.2	5	23.6	2.2	0.105	not significant
T: temperature	87.8	1	87.8	8.3	0.01	significant
F: feed rate	8.9	1	8.9	0.8	0.37	not significant
TF	14.3	1	14.3	1.4	0.26	
T^2	0.37	1	0.37	0.04	0.85	
F^2	13.1	1	13.1	1.24	0.28	

c) Response 3 : Methane concentrations statistical analysis

source	sum of squares	deg of freedom	mean square	F value	p-value, prob >F	significance
model	257	5	51.5	5.7	0.003	significant
T: temperature	130	1	130	14.5	0.0017	significant
F: feed rate	2.96	1	2.96	0.33	0.57	not significant
TF	7.52	1	7.52	0.84	0.37	
T^2	3.3×10^{-3}	1	3.3×10^{-3}	3.7×10^{-4}	0.98	
F^2	0.2	15	8.9	0.02	088	

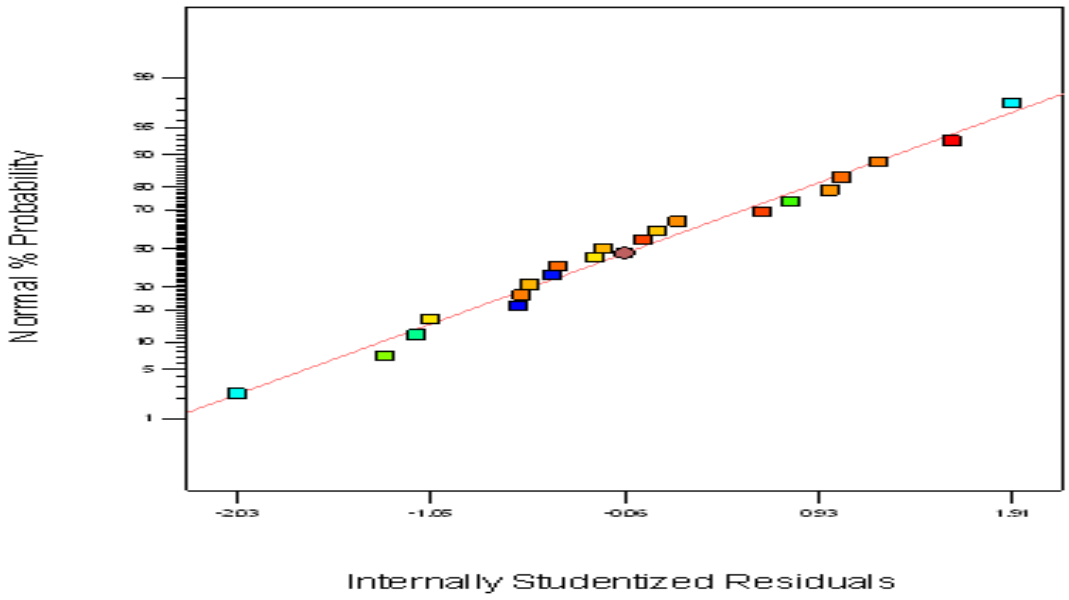

Figure 2.4 Test of normality: normal plots of the residuals

$$[H_2] = -650.7 + 1.5T + 492.7F - 0.85FT - 7.8\times10^{-4}T^2 + 217.8F^2 \quad \text{2.5}$$

$$[CO] = 209.5 - 0.49T - 135F + 1.4TF + 6.8\times10^{-5}T^2 - 1330.8F^2 \quad \text{2.6}$$

$$[CH_4] = -250.8 + 0.38T + 617.7F - 0.98FT + 6.5\times 10^{-6}T^2 + 164.4F^2 \quad \text{2.7}$$

The respective R-squared values for $[H_2]$, [CO] and $[CH_4]$ models were 0.8926, 0.4260 and 0.6574 respectively. Hence the model strength for the three syngas components could be ranked as H_2 > CH_4>CO. The equilibrium composition of the synthesis gas will depend on a large variety of complex factors determining the conversion of carbon in the gas-solid and gas phase reactions. This will include among others biomass VCM, total heat lost or gained and the overall amount of oxygen that might be present [50]. Given also the data variability that can be possible with auger based pyrolysis systems and the losses involved, these models will not be robust and typify empirical correlations in their predictive capacities.

Figure 2.5 [(a) to (c)] shows response surface curves for the range of temperature and feeding rates wherein hydrogen, carbon monoxide and methane are optimized for a

moving bed (auger) pyrolyzer. From the trend of the response surface models, it would appear that the range of temperatures and feeding rates at which the concentration of hydrogen becomes maximum does not lead to a maximum concentration of either methane or carbon monoxide or both, and vice versa.

The syngas composition [concentration (v%) ± standard deviation] of ~43.9±3.36 H_2/33.3±3.29 CO/ 20.3±2.99 CH_4 (the remainder being air that was collected into the sampling bag during analysis) was obtained for a temperature range of 740 ^oC-770 ^oC. This corresponded to the highest possible concentration for each component. At the 95 % confidence level, the confidence interval (volume %) for the respectively gases were as follows: 33.9-43.8 for H_2 with an overall data mean value of 39.1, 23.5-31.6 with an overall data mean value of 27.0 for CO and 13.9- 20.0 with an overall data mean of 19.0 for CH_4.

It is possible from the trends of the response surfaces generated that further increase in temperature could increase the concentrations of the syngas species. With a fall in the process energy efficiency with increase in temperature, further runs at higher temperatures were not justified. See Table A 1 in the Appendix for raw syngas components concentrations data. The non-conventional microwave- based method of pyrolysis gave a higher hydrogen yield (55 v%) than our results obtained using an auger conventional pyrolysis method, although the results were based on rice straw rather than an industrial sludge from paper and pulp material [16]. The results therefore compare favorably considering the established higher heat transfer efficiencies of microwave pyrolyzers versus non-fluidized fixed bed pyrolysis reactors.

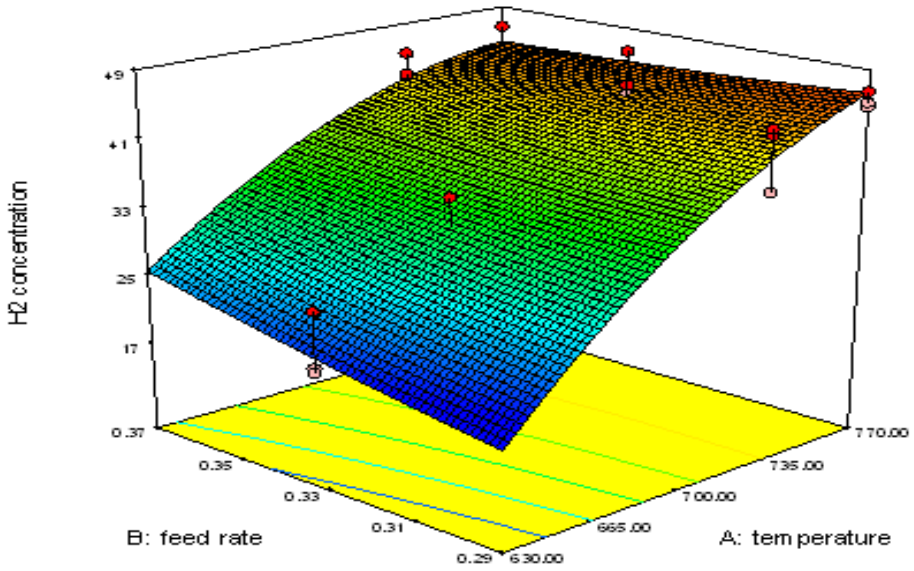

a) H_2 production as a function of temperature and biomass feeding rate

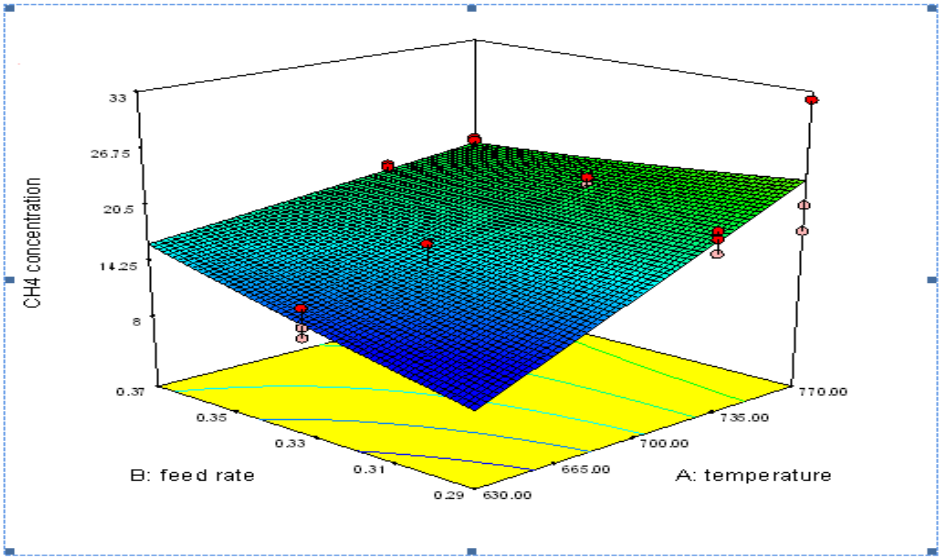

b) CH_4 production as a function of temperature and biomass feeding rate

Figure 2.5 Anova response surface models for optimum syngas compositions – a) hydrogen, b) methane and c) carbon monoxide

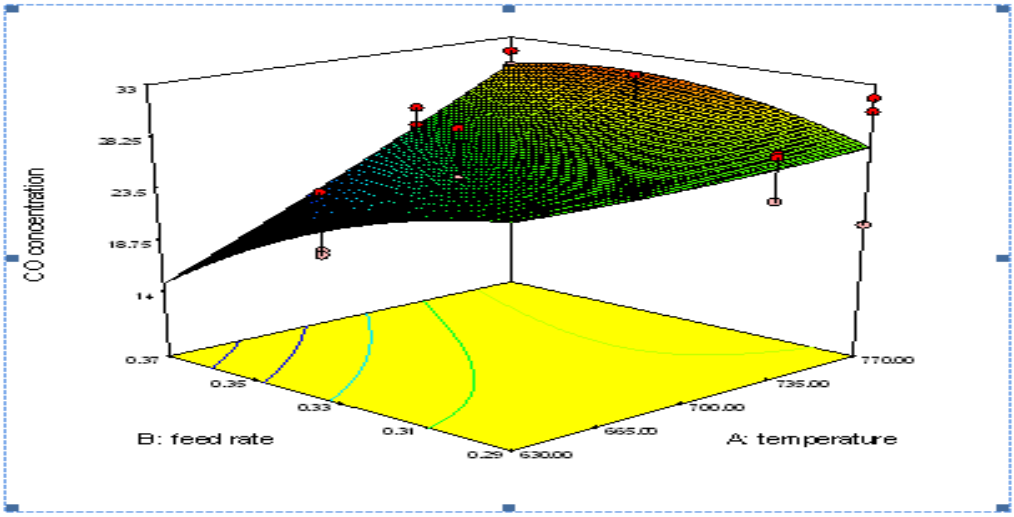

c) CO production as a function of temperature and biomass feeding rate
Figure 2.5 continued

More gas was produced as the temperature was increased due to cracking of the organic components of the bio-oil to gaseous products. The increase in the amounts of hydrogen and methane could be partly explained by the fact that some components of the organic portion of the bio-oil, such as phenols are converted into hydrogen and methane by catalytic secondary cracking reactions at higher temperatures [7,9,15]. Since elemental analysis showed the presence of alkali earth metals in the feedstock, they might be involved in the cracking of the organic fractions of the bio-oil to the respective constituents [18]. No CO_2 was detected in the chromatogram of the GC during syngas analysis. This could be explained partly by the fact that sparging with nitrogen created sufficiently oxygen-free conditions. The iron present in the biomass (0.2 wt %) together with the high temperature might have also created appropriate conditions for the catalytic steam reforming of methane and the water gas reaction (H_2O oxidation to CO and H_2) [18].

2.5.3 Overall product recovery and process efficiency

Yields and efficiencies were calculated according to definitions in Eq. 2.3-2.4. There was no correlation between char production and temperature and/or feeding rate. The % char yield (ratio of char weight to weight of sludge pyrolyzed) varied from 40.6±2.8 wt % (at 680 ^{o}C) to 51.6 ± 1.0 (at 750 ^{o}C). This could be explained by the fact that some decomposition of the biomass by micro-organisms had already taken place prior to pyrolysis at the high temperatures selected for the experiments making energy supplied at higher than 630 ^{o}C enough for carbonization.

The production of the char, bio-oil and syngas together with the change in process efficiencies with temperature is shown in Table 2.3. The overall bio-oil yield decreased from 0.18 g/kg at 630 ^{o}C to just 0.02 g/kg g at 770 ^{o}C. This was to be expected since at higher temperatures, the bio-oil is converted to gaseous products by catalytic cracking reactions. The average mass balance was approximately 84.6 wt %. This together with energy efficiency results are consistent with results obtained by Boateng et al.(2007). The raw data obtained is shown in Table A 2 of the Appendix section.

Table 2.3 Product yields and process efficiencies at all temperatures examined

temp. (^oC)	syngas L	H_2 L/kg	CH_4 L/kg	CO L/kg	bio-oil g/kg	char yield %	energy eff. %
630	231±9	21.6±4.2	13±1.8	25±3.2	0.18±2.8	46.8±3	81.2±2.6
680	237±5	34±2.2	17±1.0	28±1.8	0.16±1.6	40.6±2.8	77.2±3.8
730	384±4	76±1.6	34±0.8	47±1.4	0.05±2.1	45.2±4	70.8±1.7
750	296±9	67±4.1	29±1.8	43±3.1	0.04±1.1	51.6±1	64.7±2.8
770	243±6	50±2.7	22±1.2	35±2.1	0.02±0.8	43.8±5	57.8±5.0

Yields are based on an average of 2.2 kg of feed pyrolyzed for three replicates.

A total of 231L of syngas was produced at 630 ^oC (the equivalent of 108 ±5.7 L/ of feed). Maximum syngas production (384 L) occurred at 730 ^oC after which the total amount of gas produced decreased steadily to 243 L at 770 ^oC. Although more gas was produced as the temperature increased, the overall low energy content of the syngas contributed little in helping the energy efficiencies at higher temperatures. Also a decrease in the production of bio-oil with a relatively higher heating value helped in decreasing the energy efficiency as the process temperature increased.

The energy efficiency therefore varied from 81.2 % at 630 ^oC (where more bio-oil was produced) to just 57.8 % at 770 ^oC. Pyrolysis is an endothermic process so that when the energy needed to overcome the activation energy is supplied, any excess at higher temperatures is lost as heat to the surroundings. Therefore increases in temperature will lead to an overall fall in the energy efficiency because more electrical energy degraded to thermal energy will be needed to maintain the higher temperatures. However, since the amount of electrical energy needed to sustain the process was less than the total energy combined of the products, pyrolysis of sludge from the MixAlco

process is energy neutral. At the lowest efficiency, the total energy content of the product was ~190 % of the electrical energy input needed to sustain process.

2.5.4 Product energy distribution

Generally speaking, more than 60 % of the energy of the feedstock is lost largely to char as can be seen in Figure 2.6. While the percentage of energy stored in bio-oil is high at lower temperature that of syngas is low at lower temperature with the percentage of syngas energy at higher temperature surpassing that of bio-oil. This is because more syngas is produced at higher temperature versus bio-oil which has a relatively higher production at lower temperatures.

The energy distribution per unit mass of the feedstock for all components in the product stream is shown in Table 2.4. The impact of the decrease in the amount of bio-oil produced with increase in process temperature is reflected in the decrease in the bio-oil energy yield with increase in temperature with the bio-oil energy yield dropping from 4.3 MJ/ kg at 630 ^{o}C to 0.1 MJ/kg at 770 ^{o}C. Although more syngas is produced at higher temperatures, the energy yield associated with it is small compared to both char and bio-oil at lower temperatures. Figure 2.7 shows how the energy yields for the various syngas species vary with temperature.

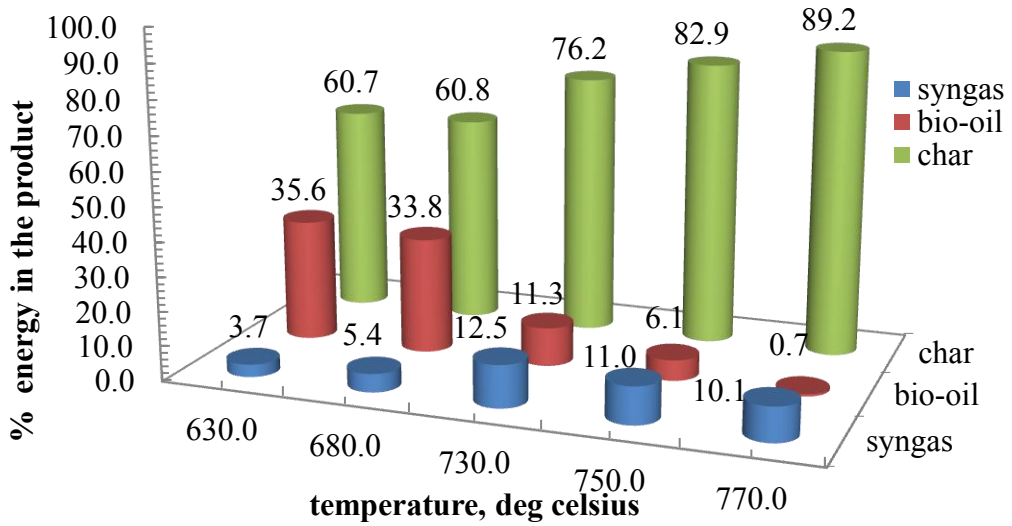

Figure 2.6 Product component energy as a percentage of total product energy

The yield of all syngas components tended to increase with temperature right up to ~ 730 ^{o}C beyond which further increase in temperature led to a decrease in the energy output per unit of feedstock pyrolyzed. This is explained by the fact that the total syngas volumetric output reached its peak at 730 ^{o}C and then decreased thereafter.

Table 2.4 Energy yield (MJ/kg sludge) and product energy distribution (%)

	energy yield(MJ/kg feed)			% energy of component		
temp.(^{o}C)	char	bio-oil	syngas	char	bio-oil	syngas
630	7.4±2.3	4.3±0.8	0.4±0.03	60.7	35.6	3.7
680	6.8±1.2	3.8±0.9	0.6±0.1	60.8	33.8	5.4
730	7.2±1.6	1.1±0.05	1.2±0.3	76.2	11.3	12.5
750	7.4±2.1	0.5±0.03	1.0±0.2	82.9	6.1	11.0
770	7.1±1.9	0.1±0.01	0.8±0.01	89.2	0.7	10.1

At temperatures between 630 to 680^{o}C syngas energy content was less than bio-oil energy content with the reverse occurring at higher temperatures. The energy contribution for each syngas species was in the order: methane >hydrogen> carbon monoxide although the component concentrations was in the order hydrogen > carbon monoxide > methane. As the temperature increased from 630 ^{o}C to 770 ^{o}C, the energy yield of hydrogen doubled from 212.5 to 505 KJ/kg due to an increase in its production at higher temperatures. A similar trend was observed for methane due partly to the fact that the higher temperature catalytic cracking of oxygenates or organic products of pyrolysis largely results in the production of methane which being a hydrocarbon has a high energy value. The energy value of carbon monoxide is the lowest of all three gases explaining why despite its higher production versus methane it still had a relatively lower energy yield.

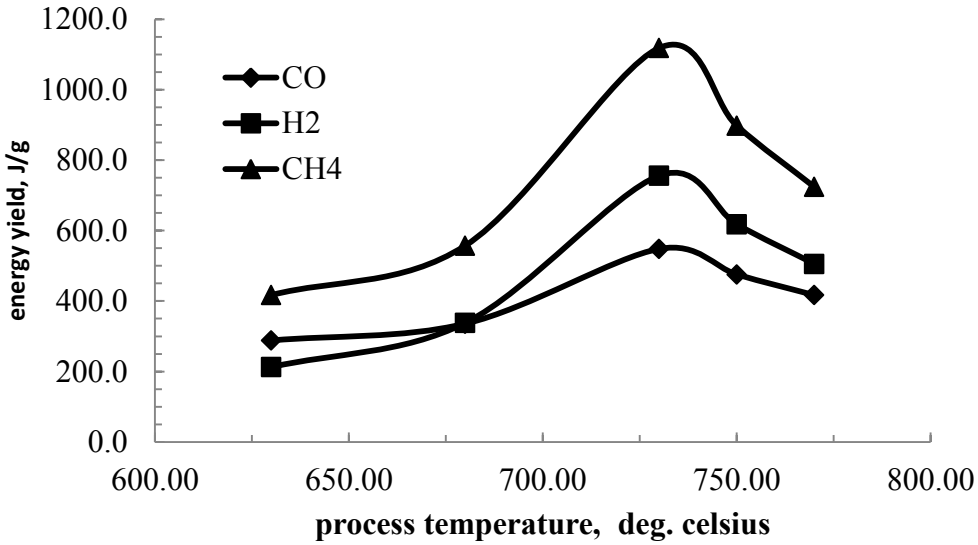

Figure 2.7 Pictorial trend for the change in energy yields of the syngas components with process temperature

2.6 Chapter Summary

In a nutshell, our results show that the sludge produced from the MixAlco process can be converted into a useful resource in the form of synthesis gas. Additionally, there is a set of temperature and /or sludge feeding rate for an auger driven pyrolyzer at which the synthesis gas can be produced with its constituents in maximum concentration. It was also found that although there was no obvious yield trend for char, synthesis gas yield increased with increase in temperature with the opposite trend for bio-oil.

Generated models for the concentrations of synthesis gas revealed approximate maximum concentrations (in volume percent) of ~43.9±3.36 H_2, 33.3±3.29 CO and 20.3±2.99 CH_4 (the remaining being air that was collected into the sampling bag during analysis) for temperatures in the range of 740-770 ^oC. At this concentration, a total of

5,990 g of H_2 with an energy content of 719.3 MJ will be produced from 1 ton of sludge pyrolyzed whose energy content is 12,441.2 MJ. The syngas with this hydrogen concentration can be passed through a pressure swing adsorption separation process to recover either pure hydrogen or a mixture of just hydrogen and carbon monoxide, both of which can be used to produce more liquid transportation fuel for the process.

CHAPTER III
PSA HYDROGEN SEPARATION FROM THE OPTIMUM SYNGAS COMPOSITION

3.1 Experimental

3.1.1 Description of setup and experimental approach

A single column PSA unit was used to simulate the performance of a two-bed PSA system. The adsorbents used were activated carbon and molecular sieve 5Å. Figure 3.1 is a schematic of the experimental setup used to do studies on impurities breakthroughs, cycle mass balances and cycle bed productivity (CBP) during runs with continuous hydrogen withdrawal.

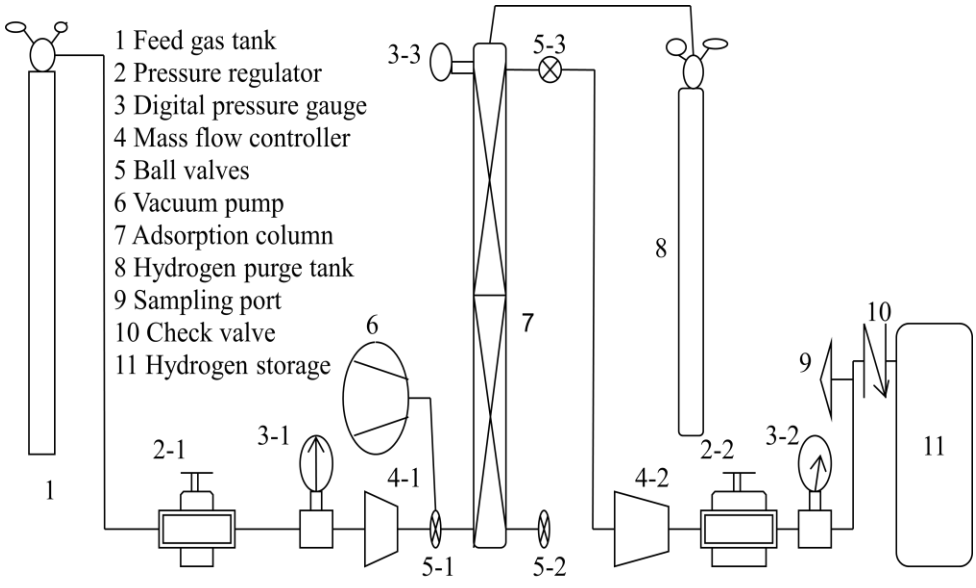

Figure 3.1 Schematic layout of the setup used in the separation of hydrogen from syngas by pressure swing adsorption

The activated carbon, a 4×8 mesh size coca 60 was supplied by Activated Carbon Corporation (Compton, California). The molecular sieve was supplied by UOP LLC (Des Plaines, Illinois). The column was a 5.0 cm internal diameter stainless steel pipe. The manufacturer reported physical properties of the adsorbents were as shown on Table 3.1.

Syngas with its components in their highest concentrations ((v/v) of 45 % H_2/35 % CO/20 % CH_4 and obtained from the pyrolysis of the MixAlco process sludge was used as the feed. The syngas was delivered from a tank into a column holding a dual bed of adsorbents, namely activated carbon (at the bottom) and molecular sieve 5Å (at the top). The feed gas went through a pressure regulator, a pressure gauge and a digital mass flow controller before entering at the bottom of the bed. At the top, another pressure gauge was installed to measure potential bed pressure drop.

Table 3.1 Physical properties of adsorbents – manufacturers' report

properties	5Å (1/16" pellets)	activated carbon (granular)	unit
specific surface area	-	1200	m^2/g
bulk density	0.71	0.47	g/cc
moisture content	1.0	2.0	wt %
min. CCl_4 activity	-	60	-
ash content	-	3.0	wt %
particle diameter	0.16	-	cm
ater capacity	21	-	wt %

To maintain the bed pressure, the exit gas flow was controlled by a digital hydrogen mass flow controller. The feed gas pressure was regulated using a pressure regulator supplied by McMaster-Carr (Aurora, Ohio). The effluent gas pressure and the pressure dynamic of the bed were read from digital pressure gauges supplied by Cole-

Parmer (Vernon Hills, Illinois). The feed flow was then controlled by a programmable digital mass flow controller supplied by Alicat Scientific (Tucson, Arizona). Downstream the column, a ball valve, the same mass flow controller and pressure gauge (in make and manufacturer) were installed.

Separation and recovery of hydrogen from impurity carbon monoxide and methane was through a series of cycle steps such as pressurization with feed (with no hydrogen discharged), pressurization with feed (with hydrogen discharged), co-current depressurization, counter-current depressurization and external purge with hydrogen, described in detail in an appropriate section. Experiments to determine cycle recoveries from cycle bed productivities for three different adsorbent amounts were preceded by preliminary experiments to test separation effectiveness of selected adsorbent pair.

3.1.2 Preliminary experimental runs

Syngas feed flow rate was studied at two levels – 7.0 and 10.0 standard lpm while the pressure was studied at three levels – 310, 610 and 710 kPa in 15 experimental runs. A 200 cm stainless steel column was first filled to 120 cm with 1,585 g of activated carbon, and then was topped with 1,307 g of molecular sieve 5Å. The adsorption column was pressurized until a predetermined pressure was reached. At that pressure, sampling port 9-1 was opened and the effluent analyzed using an SRI 8610C GC supplied by SRI Instruments (Torrance, California).

A random factorial experimental statistical design using the Design Expert software was performed for all combinations of feed rate and pressure to study the impact of each input parameter on traditional output parameters such as hydrogen purity (%), hydrogen recovery (%) and hydrogen discharge rate (standard lpm). Experiments were performed in triplicates for each combination of feed flow and pressure with the intention of selecting the feed rate and pressure that gave the best hydrogen purity and per-pass recovery for use in actual experiments meant to efficiently recover hydrogen from the syngas with the specified composition. 15 out of a full factorial total of 18

experiments were performed. The Design Expert software was used to analyze the data obtained.

3.1.3 Investigative experiments using three different adsorbent amounts

Because of the positive influence of pressure and feed rate on the discharge rate and % recovery, a higher pressure of 8.0 atm and a mass flow controller full range feed rate of 10 standard lpm were therefore selected to conduct separations in continuous run mode for the purposes of determining impurity breakthrough times (from breakthrough curves), cycle mass balances and bed productivities at a constant hydrogen draw rate of ~4.5 standard lpm. This draw rate was selected because it approximately balanced the rate at which hydrogen was fed into the bed, giving a constant pressure dynamic condition. A total of 9 experiments, in triplicates (to determine breakthrough times for impurities CO and CH_4) were then performed using 200 cm, 135 cm and 70 cm columns each containing 2,892 g, 1,962 g and 1,013 g of adsorbent respectively with a feed rate of 10 standard lpm and 809 kPa pressure. Another 9 experiments, in triplicates were performed at the same condition of pressure, flow rate and adsorbent amounts to carry out cycle mass balances and hence determine cycle recovery and cycle bed productivities but with the times for pressurization (with hydrogen discharge) being less than the breakthrough times to prevent the Co and CH_4 impurity front from reaching the top of the column. The stated hypothesis (H) goes thus: *There is an optimum CBP (corresponding to a given adsorbent amount) for a ½ cycle. Consequently, basing cycle recovery on the CBP can be a better method for assessing PSA cycle performance.*

3.1.4 Cycle description and breakthrough times

In order to characterize pressure drops in dynamic systems Sundaram and Wankat (1988) combined Darcy's Law with the continuity equation and then arrived at a

characteristic dimensionless constant,ζ, which varies inversely with the column length. Their rule of thumb was that, for values of ζ greater than 0.5, the pressure drops can be assumed insignificant. PSA beds can be run under dynamic or static conditions, and the selection of ζ may become relevant in dynamic systems. For $\zeta < 0.5$, a certain bed height results in significant pressure drop limiting impurities adsorption and breakthrough time.

The value of ζ was not specifically determined although experiments were performed under dynamic conditions. To account for this, breakthrough times were determined for each adsorbent bed height or adsorbent amount used and cycle mass balances were conducted for pressurizations step with durations less than the breakthrough time for each bed height or adsorbent amount. Large adsorbent particle sizes minimized bulk mass transfer limitations hence eliminating pressure drop across the beds. A robust dynamic pressurized bed was obtained with an inlet pressure of 8.2 atm and a nearly constant bed pressure of 8 atm.

The effluent leaving port 9-2 was analyzed at specific time intervals until CO and CH_4 exited column. With all pressure units in atm, the cycle steps employed in cycle mass balance and CBP estimations were:

1 A pressurization with feed synthesis gas (with no hydrogen leaving bed) from atmospheric pressure to a pressure of 809 kPa.
2 A continuous pressurization at 809 kPa with feed (as hydrogen was discharged at the top of the column).
3 A co-currrent depressurization from (from 809 kPa to 379, 448 and 482 kPa respectively for 200 cm, 135 cm and 70 cm beds). During this step, there was no feed stream but with hydrogen released at the top of the bed. The hydrogen from steps 2 and 3 were collected into the storage tank and later wasted.
4 Acounter-current depressurization further decreased the bed pressure to 101 kPa.
5 Pure hydrogen was delivered counter-currently (through valve 5-3) from the hydrogen purge tank and then used to pressurize the bed from 101 kPa to 310 kPa.
6 The bed pressure was finally reduced to 101 kPa by opening valve 5-2. The effluents of steps 4 and 6 were wasted by directing to the outside through the fume hood.

The overall cycle times for the 200, 135 and 70cm columns each holding a total of 2892 g, 1962 g and 1013 g of adsorbent respectively were 23.8, 16.3 and 7.8 minutes. Step 2, continuous pressurization at 809 kPa took place for a total time that was less than the breakthrough time (t_{br}) at which the impurities (CO and CH_4) brokethrough to prevent the impurity front from reaching the top of the column. The time in steps 1 and 2 were combined to get the time during which hydrogen was fed into the columns.

Figure 3.2 is a pictorial schematic of a two-bed PSA system based on a half cycle on bed 2 (complete cycle on bed two only). Bed 1 undergoes a blowdown (release of column contents) followed by external purge with molecular hydrogen. At the same time, bed 2 initiates and undergoes pressurization to a predetermined operational pressure, followed by pressurization with feed during which impurities adsorb on the bed. During this step pure hydrogen is discharged at the top of the bed with simultaneous use of the hydrogen in the purge step of bed 1 (in the case of internal purge with hydrogen). Bed 2 then undergoes blowdown (by way of co-current and counter –current depressurization/desorption). At the end of the blowdown, bed 2 is then purged to be ready for the next half cycle after bed 1 completes its own next half cycle. The cycle steps are phased out for continuous discharge of pure hydrogen. We used the half cycle steps detailed in Figure 3.2 on bed 2 to purify hydrogen and performed a half cycle mass balance that was used to calculate cycle bed productivity for a 2-bed PSA system. A detailed cycle step timing data are shown in Table 3.2.

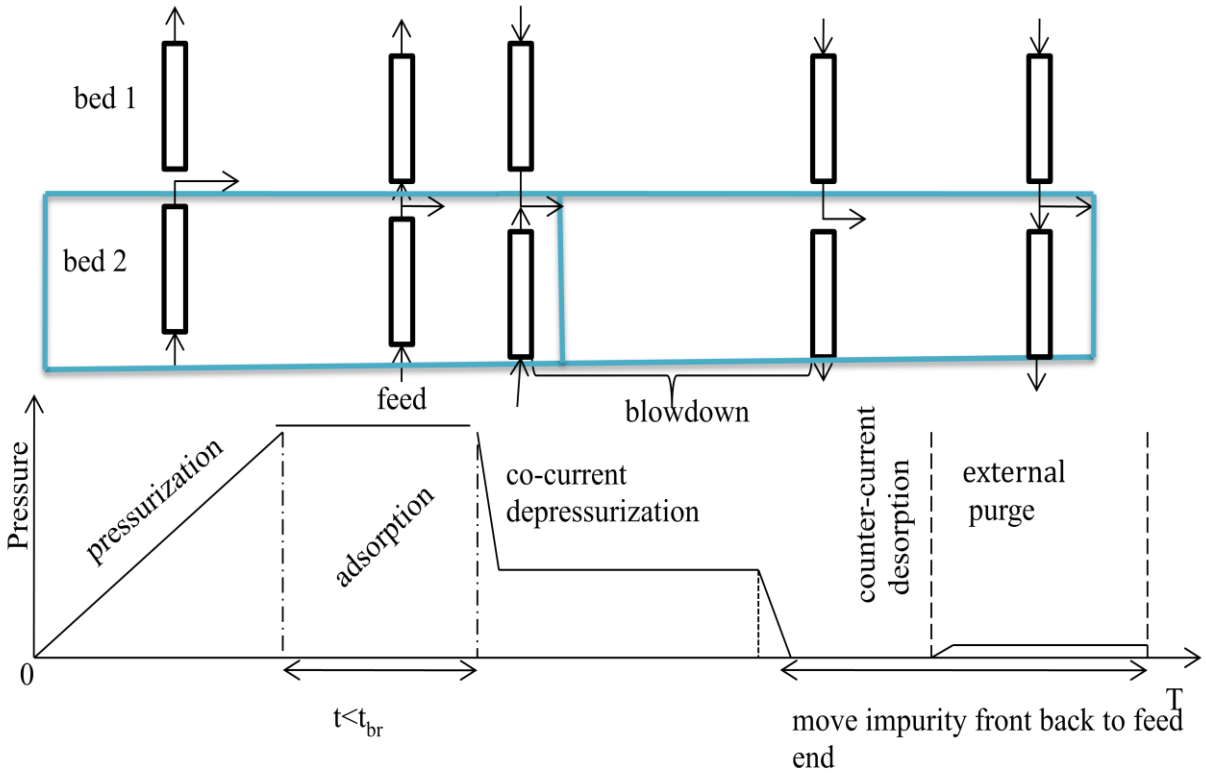

Figure 3.2 Half cycle steps on bed 2 for a two-bed PSA system

Table 3.2 Cycle steps, times (minutes) and pressure changes (atm) for the three adsorbent amounts

column	time							
height (cm)	1	2	3	4	5	6	7	B*
200	7.7	12	3.3	0.2	0.3	0.3	23.8	15.0
135	4.6	9.0	2.2	0.2	0.2	0.2	16.3	11.2
70	2.4	4.0	1.0	0.2	0.1	0.1	7.8	4.4
pressure changes (atm)								
200			8.0-3.9	3.9-1.0				
135			8.0-4.6	4.6-1.0	1.0-3.2	3.2-1.0		
70			8.0-5.0	5.0-1.0				

1=pressurization with feed (no discharge); 2 =co-current pressurization (with discharge); 3=co-current depressurization; 4=counter-current depressurization; 5= H_2 pressurization 6= H_2 purge; 7= cycle time; B=t_{br} (for CO and CH_4)*

3.1.5 Parameter estimation

The percent per-pass recovery and purity were as defined in Equations 3.1 and 3.2 for initial experiments performed on the 200 cm column with 2,893 g of adsorbent. This definition of recovery is in accord with the traditional definition of the product recovery where the flow rate of the raffinate product is expressed as a percentage of the flow rate of the feed stream for the desired product. The hydrogen discharge rate was characterized by the rate at which hydrogen exited the top of the column at the maximum set pressure. See numerator of Equation 3.1. Since this rate increases with increase in the bed pressure, the value at the maximum pressure was the maximum hydrogen discharge rate.

$$\text{per-pass recovery (\%)} = \frac{\text{max } H_2 \text{ flow rate (mg/s) in product stream}}{\text{total feed flow (mg/s)} \times \text{hydrogen feed concentration}} \times 100 \ldots..3.1$$

$$\text{purity (\%)} = \frac{\text{conc. of } H_2 \text{ in the product stream (v\%) at sampling time}}{\text{sum of the individual conc.of species in the product stream (v\%)}} \times 100 \ldots..3.2$$

In order to perform cycle mass balances for the respective bed heights/adsorbent amounts, the beds were pressurized to 8.0 atm at a feed rate of 10 standard lpm. This was followed by co-current pressurization but with hydrogen released. The combined time for these pressurization steps was useful in calculating the hydrogen "mass in". The hydrogen "mass out" was obtained from the hydrogen discharge rate and the time in steps 2 and 3.

To get the actual hydrogen mass in or out, a plot of hydrogen flow rates versus time was obtained and the Matlab software was used to calculate the total area by the Trapezoidal Rule ("trapz" function). This was numerically equal to the volume of hydrogen discharged over the respective times in the relevant cycle steps. The product of the density of hydrogen at standard conditions and the discharge rate gave the mass flow rate of hydrogen out. With focus on the amount of hydrogen discharged the hydrogen

adsorption or accumulation on the adsorbent pores was considered as losses and ignored largely because of the difficulties associated with measuring with accuracy the flows of gas mixtures with varying compositions. The terms in the mass balance are shown in Equation 3.3 while the definitions of cycle recovery (%) and cycle productivity are shown in Equations 3.4 and 3.5 respectively. The error margins per cycle of both the mean mass of hydrogen discharged, and of the recovery (%) for each bed height or adsorbent amount was within 4.0 %.

cycle mass of hydrogen out (g) = cycle mass of hydrogen in (g) -cycle mass of hydrogen lost to the adsorbents (g).....3.3 (a)

$$\rho Q\,(\text{out}) \int_0^t p\,dt = \text{ø}\rho Q\,(\text{in}) \int_0^t dt - \text{cycle mass of hydrogen lost} \ldots\ldots\ldots\ldots\ldots\ldots\ldots\ldots 3.3\ (b)$$

$$\%\ \text{cycle recovery} = \frac{\text{mass of hydrogen caught per cycle}}{\text{mass of hydrogen fed per cycle}} \times 100 \ldots\ldots\ldots\ldots\ldots\ldots\ldots\ldots 3.4$$

$$\text{cycle productivity}\left(\frac{\text{mg}}{\text{g}}\right) = \frac{\text{mass of hydrogen caught per cycle}}{\text{combined weight of adsorbents}} \ldots\ldots\ldots\ldots\ldots\ldots\ldots\ldots 3.5$$

3.2 Results and Discussion

3.2.1 Preliminary experiments on 2,892 g of adsorbent

The Design Expert generated summary results for all combinations of input parameters during preliminary screening experiments for the 200 cm (2,892 g of adsorbent) bed are shown in Table 3.3. The mean values of the three parameters were as follows: % purity (99.9), % recovery (55) and discharge rate (2.1).

This means that a little over half of the hydrogen in the feed stream will be recovered as the product with the balance lost to the adsorbent matrix. This translates to

a mean hydrogen discharge rate of 2.1 standard lpm across the range of pressures and feed rates studied. The productivity (L/kg) increased with bed pressure and feed rate from 35.2±4.4 at 3 atm/45 psig and 7slpm to 1270.2±35.4 standard lpm/kg of adsorbent/minute at 7 atm/102 psig and 10 standard lpm.

Table 3.3 Summary results for runs on 2,892 g adsorbents

response	name	units	analysis	min	max	mean	std	model
Y_1	purity	%	factorial	99.9	99.9	99.9	0	2 factor
Y_2	recovery	%	factorial	22.7	85.6	55.0	25.3	2 factor
Y_3	discharge	slpm	factorial	1.0	3.9	2.1	2.1	2 factor

The results showed that the composite adsorbent bed can be used to separate hydrogen from a low hydrogen concentration pyrolysis gas stream with hydrogen, methane and carbon monoxide at their optimum production concentrations (v/v) of 45 % H_2/ 35 % CO/ 20 % CH_4 to a 99.9 % H_2 purity. The variations in the output parameters with changes in the input parameters are shown in Figure 3.3. Both high pressure and feed flow rate improved the percent recovery and discharge rate as shown in Figure 3.3. Since 15 out of 18 possible factorial experiments were performed (excluding the triplicate from the condition of 7 standard lpm and 710 kPa), the point on Figure 3.3 for this condition is a poorly predicted non-experimental point and was considered as an outlier. This is evident by the fact that, unlike other points, this point lacks an error bar.

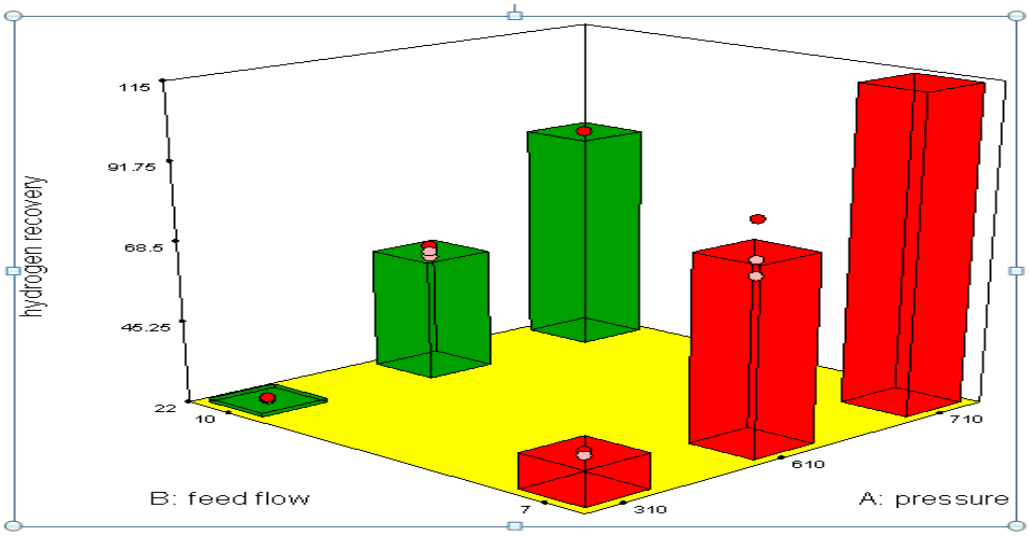

a) Change in the % recovery with feed flow and pressure (kPa)

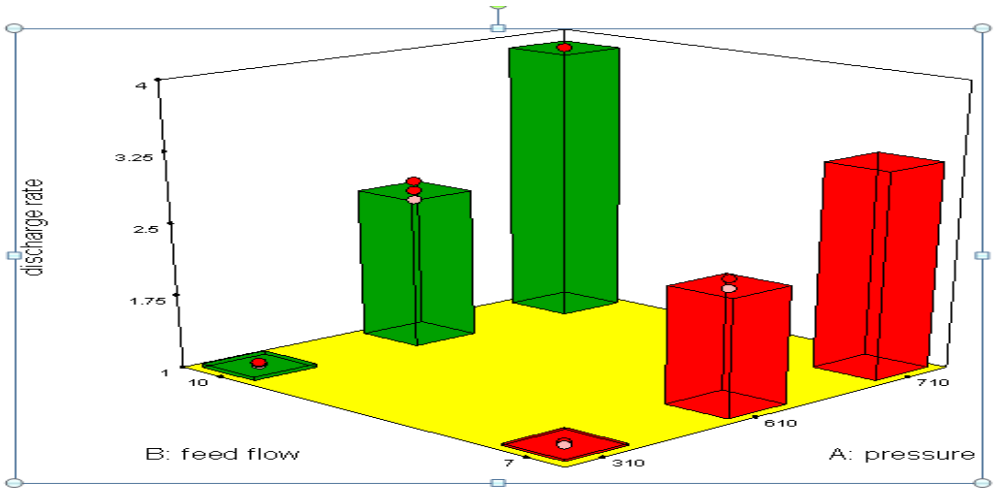

b) Change in H_2 discharge rate with pressure (kPa) and feed flow

Figure 3.3 Changes in % recovery and throughput with changes in feed flow rate (slpm) and bed pressure (kPa) – a) [% recovery]; b) [discharge rate (slpm) of hydrogen produced]

The two factors studied, the interaction between them and the generated model were statistically significant (p-value <<0.05) as factors affecting recovery and discharge rate. For a given feed rate, the percent recovery and discharge increased with increase in bed pressure, but the increase in recovery seemed to be less at higher feed rates compared to lower feed rates for a given bed pressure. The bar heights represent predicted mean values from a software generated best fit-model.

Yang et al. (2009) studied the dynamics of bed recovery using superficial velocity, rather than feed flow. Arriving at the same conclusion, they explained the fall in recovery with increase in superficial velocity by arguing that there is a broadening of the mass transfer zone with increase in feed rate or superficial velocity. For a given pressure, increasing the feed flow (superficial velocity) reduces the residence time of the least strongly adsorbed desired H_2, thereby reducing the impact of H_2-co-adsorption on the adsorbent. Higher pressures means an increase in the concentrations of CO and CH_4 each having a higher affinity for adsorbent. Both compete more favorably with H_2 as the number of H_2 adsorption sites is reduced. This leads to more enriched hydrogen leaving the top of the column. Our result of an increase in recovery at higher pressure is explained by the pressure dependence of PSA separation in both Knudsen and bulk molecular diffusion models for hydrogen [Poisseuille Equation, 3.8].

3.2.2 Breakthrough curves and breakthrough times

The effluent concentrations of hydrogen, methane and carbon monoxide are shown in Figure 3.4. Figure 3.5 shows the hydrogen purity time profile for the three column heights each holding a different amount of the 2 adsorbents investigated with the actual volumetric flow rate (or discharge rate) being the product of the constant discharge rate of 4.5 standard lpm and the percent purity of hydrogen. The breakthrough times (reported with standard errors of the means and as deduced from the impurity gas concentrations profile curves) and H_2 recovery (from areas under the discharge vs time curves) are summarized in Table 3.4.

Table 3.4 Performance data for the 3 adsorbent amounts (10 slpm and 8 atm)

bed height (cm)	adsorbent height in bed (cm)	adsorbent type	adsorbent weight (g)	H_2 mass in (g)	H_2 mass out (g)	Cycle recovery (%)	impurity breakthrough time (min.)
200	120	AC	1585	7.9	5.7	72.2	14.95±2.1
	80	5Å	1307				
135	73	AC	1067	6.7	4.4	65.4	12.35±1.0
	62	5Å	896				
70	38	AC	555	2.6	1.6	60.2	5.4±1.3
	32	5Å	458				

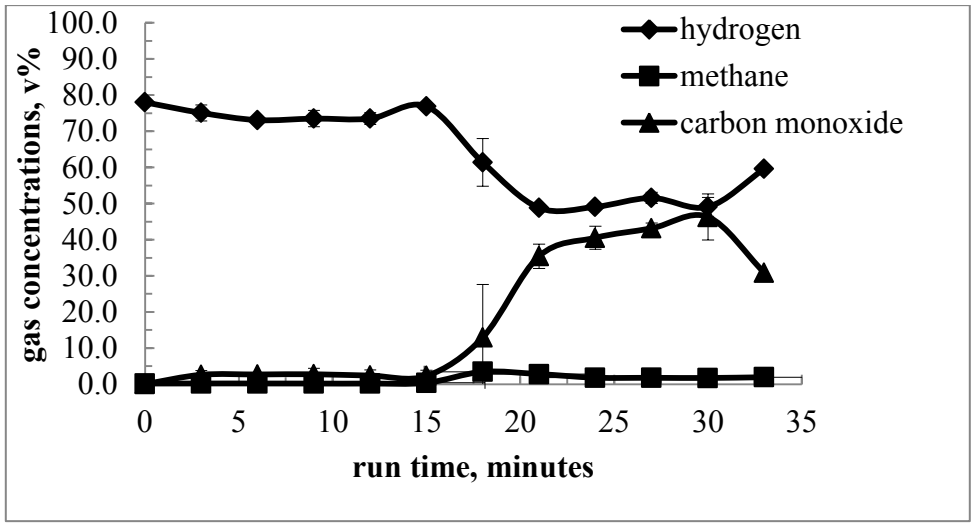

a) 2,892 g of adsorbent

Figure 3.4 Concentrations of product gas streams against time of run at 8.0 atm for a feed rate of 10 slpm: a) 2,892 g, b) 1,962 g and c) 1,013 g of adsorbent used

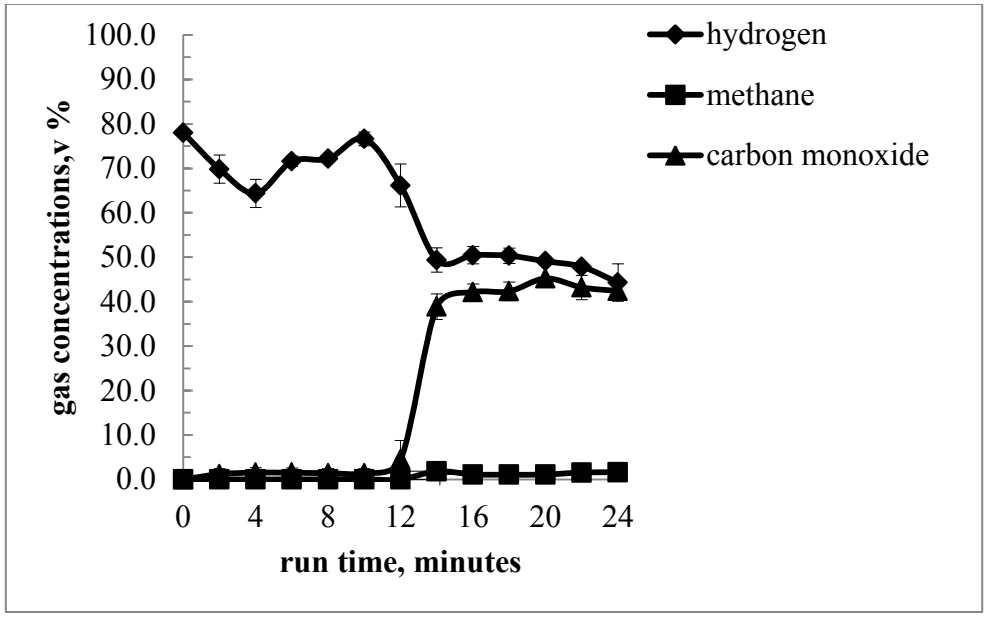

b) 1,962 g of adsorbent

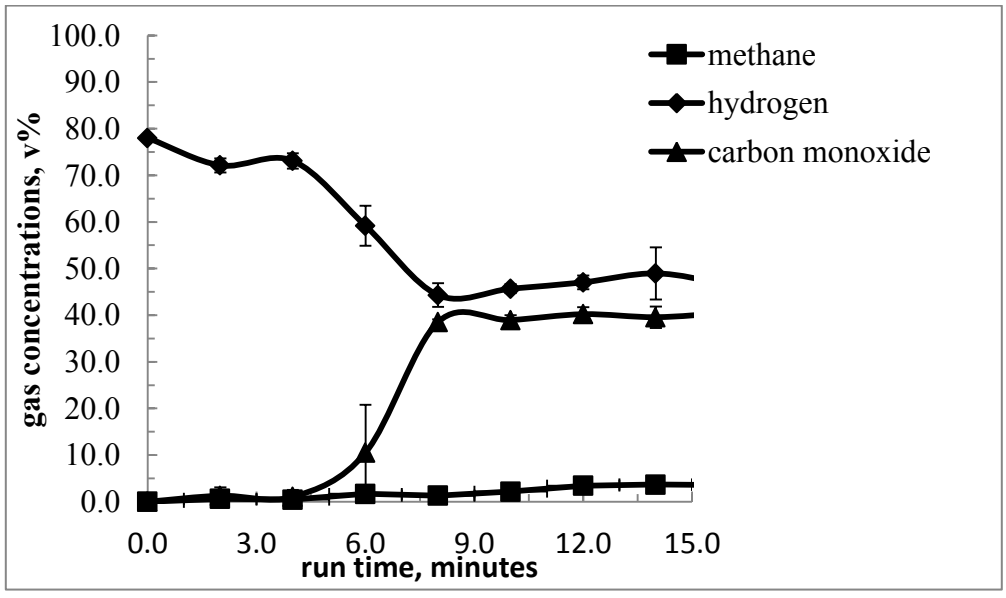

c) 1,013 g of adsorbent
Figure 3.4 continued

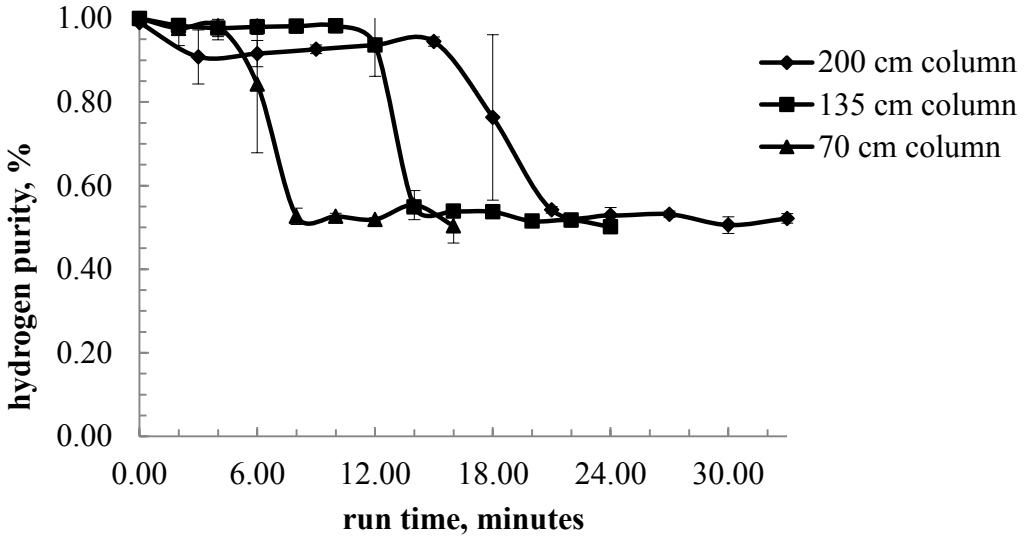

Figure 3.5 Hydrogen purity versus run time

It should be noted that, the concentrations of the three gases (together with those of O_2 and N_2 carried over in the sampling bag during gas sampling) added to 100. From curves in Figure 3.4 and Figure 3.5, the smaller the adsorbent amount, the shorter the breakthrough time (t_{br}) for CO and CH_4 for a given flow. Hence the greater the amount of adsorbent used, the better the separation, and the % recovery.

In PSA beds, the dynamics of kinetically and thermodynamically controlled physi-sorption interactions of the adsorbates with the adsorbent surface creates three distinct zones along the length of the adsorption bed. When the fresh feed gets into the bed, the impurity front generated under pressure is largely a saturated zone. Further down the middle of the bed, a concentration gradient between the gas phase inside the pores and the pore surfaces creates a mass transfer zone. The bed terminates with a fresh zone of unsaturated adsorbent at the top. Separation always aims at pushing the mass transfer zone away from the top of the column at the end of each ½ cycle to reduce the partial pressure of the impurities in the bed. This enhances the % purity.

In terms of critical diameter the ranking for methane, carbon monoxide and hydrogen is as follows: methane > carbon monoxide > hydrogen. While the pore structure of activated carbon is unimodal, that of molecular sieve (5Å) is bimodal with microspores interconnected by macropores. The size of hydrogen and to some extent that of carbon monoxide permit their mass transfer flux to be largely dominated by both bulk molecular and Knudsen diffusion (through activated carbon and 5Å molecular sieve) according to Equations 3.6 and 3.7.

$$D_m \propto \frac{T^{1.7}}{P\sqrt{M}} \quad \ldots\ldots 3.6$$

$$D_K \propto r\sqrt{T/M} \quad \ldots\ldots 3.7$$

Recovery of hydrogen at lower pressures is largely due to faster bulk molecular diffusion through both adsorbents. Larger molecules such as CO and CH_4 move slowly by Knudsen diffusion through the pores especially at lower pressures. The flux of each adsorbate moves at a different rate (and hence breakthrough at different times) due largely to differences in molecular weight. In the intermediate mass transfer region, mass flux in PSA is governed more by the equivalent Poiseuille diffusivity that depends largely on pressure since the influence of viscosity is undermined by the minimal differences in the viscosities of the gases under the same conditions of temperature and pressure. Hence improved recovery is obtained at higher pressure as illustrated in Poiseuille Equation:

$$D = \frac{Pr^2}{8\mu} \quad \ldots\ldots 3.8$$

The persistent micropores in unimodal adsorbents such as activated carbon and in bimodal heterogeneous zeolites such as 5Å create a medium for micropore diffusion for each adsorbent. In micropores mass transfer is largely dependent on differences in concentration gradients and steric hindrances or activation energy barriers arising from different kinetic diameters of the molecules. For a given micropore channel, only species

with a given critical diameter will move across and be separated, because they experience low steric hindrance. Those with larger critical diameters experience higher steric hindrances, requiring a higher activation energy. The channels of zeolites therefore kinetically and selectively sieve out only smaller critical diameter molecules.

3.2.3 Hydrogen recoveries and cycle bed productivities

As can be seen from Table 3.4, decreasing the adsorbent amount from 2,892 to 1,962 g caused the recovery to dive from 72.2% to 65.4 %. A further decrease to 1,013 g caused the recovery to fall almost 60 %. This could be explained by a reduction in the retention time for CO and CH_4 removal from the gas phase with decreasing bed volume. An increase in the retention time has been shown to boost recovery, Yang et al. (2009). The areas under the graphs in Figure 3.6 represent the mass of hydrogen recovered per cycle. This area increased with increase in the amount of adsorbent used, and hence an increase in the amount of H_2 discharged at the end of the cycle.

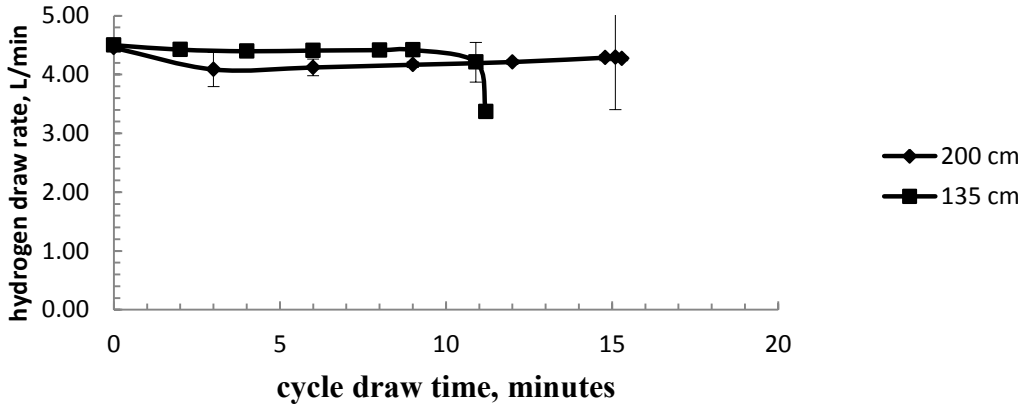

a) 2,892 g adsorbent (200 cm bed) and 1,962 g of adsorbent (135 cm bed)

Figure 3.6 Cycle hydrogen discharged versus separation time: a) 2,892 and 1,962 g, b) 1,013 g of adsorbent

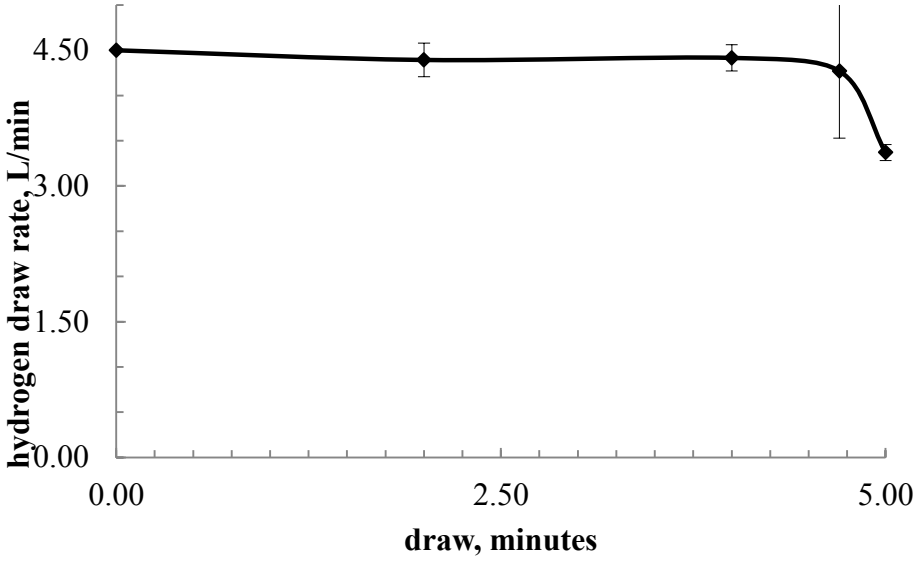

b) 1,013 g of adsorbent (70 cm bed)
Figure 3.6 continued

Figure 3.7 shows that although the cycle recovery seems to increase with an increase in bed height and hence amount of adsorbent needed, the cycle bed productivity (CBP) maintained that trend only to a certain adsorbent amount beyond which it (CBP) peaked, and then decreased with increasing adsorbent amount. The experimental data fits a polynomial model neatly. Maximum cycle productivity (2.25 mg/g adsorbent) occurred for an adsorbent amount of ~2,300 g.

A relatively low hydrogen concentration synthesis gas stream is produced from the pyrolysis of biomass compared to the amount of hydrogen generated from say industrial steam reforming of methane followed by the water-gas-shift reaction. From base experimental data the projected syngas production was up to 95,160 g (2,434.7 MJ) per ton of MixAlco sludge pyrolyzed. This translates into 5,990 g H_2, 65,000 g CO and 21,170 g CH_4 produced at optimum condition. From Figure 3.7 maximum CBP gives a cycle bed recovery of 66.2 %. This translates to 3,965 g H_2 or (476.2 MJ) per ton of MixAlco process sludge available for its hydrogenation unit operations to produce more gasoline, JP8 and diesel. The figure also shows that cycle bed productivity can be a more

cost effective way of assessing PSA performance because although cycle recovery actually increases, after the maximum CBP of 2.25 mg H_2/g of adsorbent (for 2,300 g of adsorbent) is attained, a higher cycle recovery of 72 % (past maximum CBP) actually corresponds to a lower CBP of 1.8 mg H_2/g. It would appear % recovery is a weaker evaluation metric. Hence a stronger metric with cost implications is the CBP, which can be used in assessing PSA bed performances in multi-bed PSA systems. This is because it directly relates to the amount of adsorbent, and hence the total cost associated with product recovery especially for low hydrogen concentration feed streams.

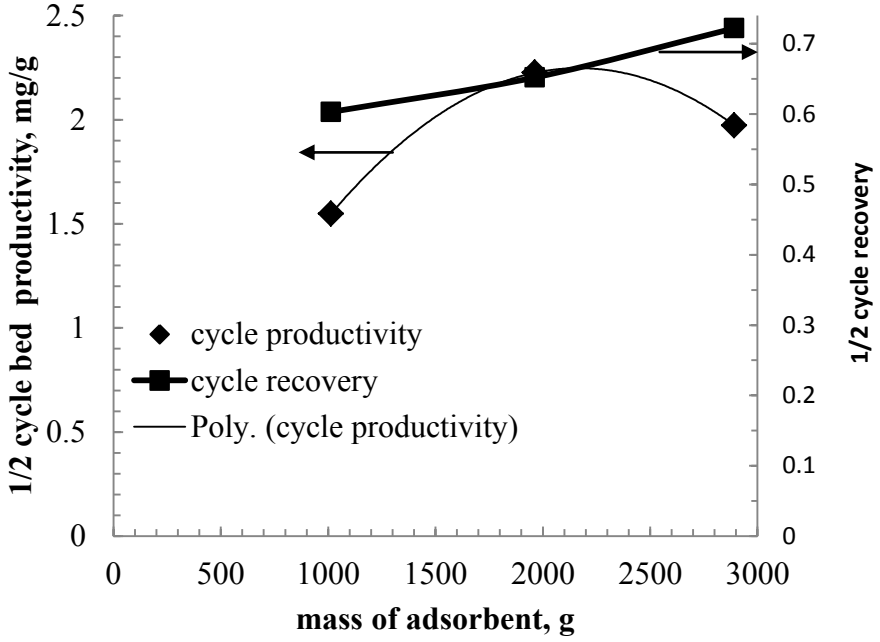

Figure 3.7 Effect of adsorbent amount on PSA bed productivity

3.2.4 Integrating pyrolysis and PSA for optimum hydrogen recovery

The product gas is usually needed to provide the needed pressure in the next pressurization step in vessels that previously underwent a blowdown in PSA systems with a cascade of vessels in series. It is for this reason that one of the requirements is that the product species to be captured should be in a higher concentration in the feed streams, preferably in excess of 65 v% [37]. The primordial PSA system was the Skarstrom system with two beds alternately undergoing pressurization and depressurization in a single cycle [19]. Many modifications to this system have resulted in the connection of multiple beds in series to improve percent recovery and purity. While this is difficult with low concentrations of the desired species in the feed stream, such multiple cascading of the beds results only in a slight increase in the percent purity although an increase in recovery of about 50 % has been reported [38].

Figure 3.8 shows how combining a PSA system with optimum bed productivity could be used to harness hydrogen produced from relatively lower hydrogen concentration sources such as ones derived from the pyrolysis of MixAlco process

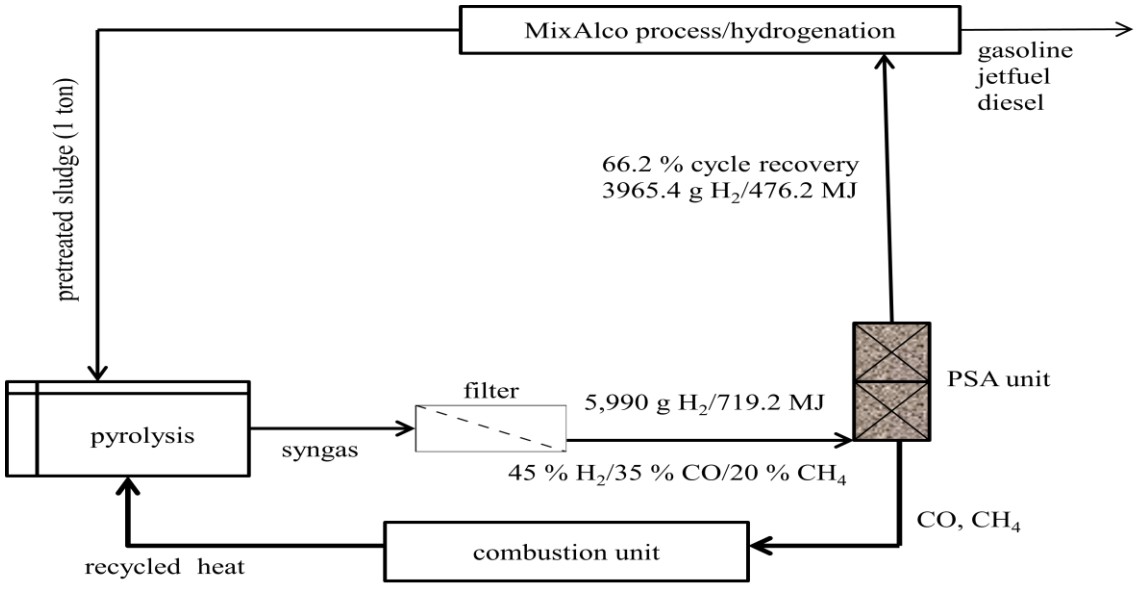

Figure 3.8 Efficient integrated hydrogen recovery for use in the MixAlco process

sludge to increase yields of liquid transportation fuels. At our experimental conditions, for each ton of sludge pyrolyzed, the PSA will recover up to 3,965.4 g of H_2 gas for 5,990 g of H_2 supplied at optimum syngas composition (43.9±3.36 v % H_2/33.3±3.29 v % CO/20.3±2.99 v % CH_4) at 740 ^oC for an optimum CBP of 66.6 %. The energy equivalent of this hydrogen will be approximately 476.2 MJ. Hence selecting the adsorbent amount that leads to optimum CBP will lead to an improved hydrogen recovery with yet a minimum number of beds versus the multiple beds used for product recovery in PSA systems with the attendant costs.

3.3 Chapter Summary

Only about 44.3 v% hydrogen was obtained from the syngas obtained from the pyrolysis of the MixAlco sludge process. Hence efficient hydrogen separation is necessary because the concentration of hydrogen from this source is low compared to the stoichiometric value of 75 v% obtained from the industrial steam reforming of methane. A method was developed to efficiently separate hydrogen from the synthesis gas obtained from the pyrolysis of the sludge derived from the MixAlco process. The method developed was based on cycle mass balances and determined the PSA % cycle recovery using another parameter called the cycle bed productivity.

It was found that while the % recovery will increase with an increase in the amount of adsorbent used, the cycle bed productivity declined after its maximum value as the amount of adsorbent increased. A cycle bed productivity of 66.2 % will mean that up to 3,965.4 g (476.2 MJ) of hydrogen will be recovered for every 5,990 g (719 MJ) of hydrogen in the feed stream [obtained from 1.0 ton (12,441.2 MJ) of MixlAlco sludge pyrolysed]. Using the traditional % recovery value of 72.2 % led to a higher amount of hydrogen recovered, but the amount of adsorbent used increased by ~22 %.

CHAPTER IV
CATALYTIC CONVERSION OF MIXALCO PROCESS DERIVED SYNGAS TO LIQUID FUELS

4.1 Description of Setup

The feed synthesis gas was derived from the pyrolysis of sludge obtained as the by-product of the MixAlco process. This syngas was originally produced with an approximate H_2:CO ratio of 1.3. The schematic of the process used for the catalytic conversion of the syngas to transportation fuels is diagrammed in Figure 4.1.

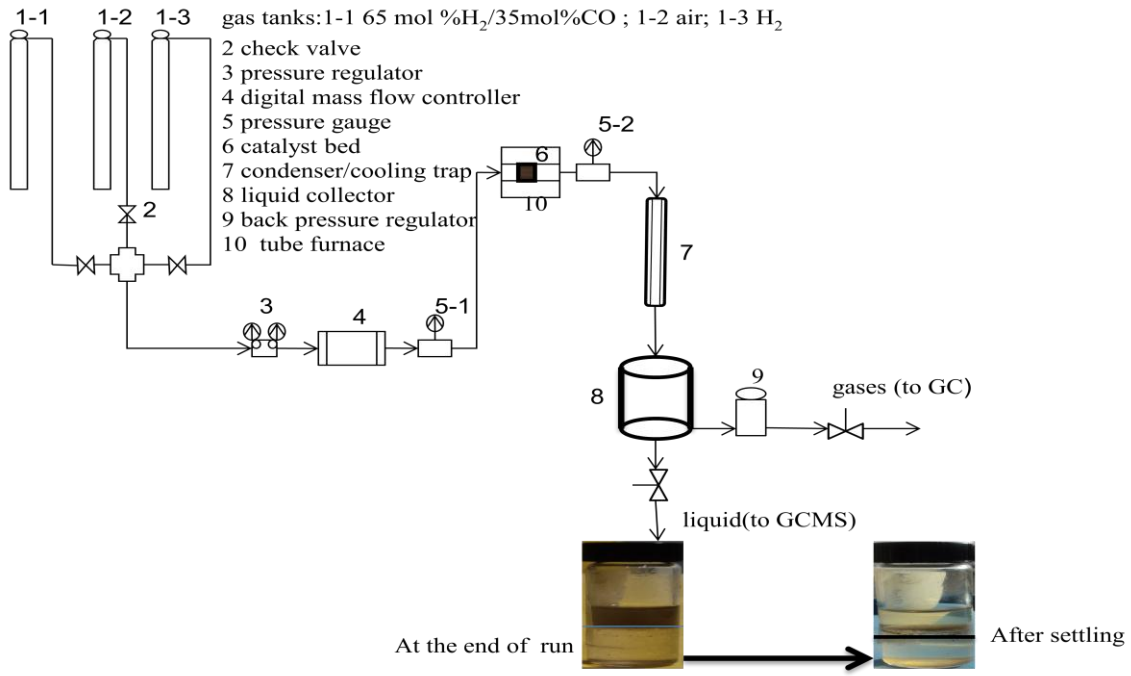

Figure 4.1 A schematic representation of the setup for the catalytic conversion of syngas to liquid hydrocarbons

Three gas tanks (one with pure air, another with pure hydrogen and a third containing a 65 mol % H_2/35 mol % CO syngas mixture, after adjustment of H_2:CO

ratio) were connected to a catalyst bed via a pressure regulator (Air Gas, College Station, Texas), a mass flow controller (Alicat Scientific, Tucson, Arizona) and a pressure gauge (McMasters Carr, Aurora, Ohio) respectively. The catalyst was heated electrically in a horizontal tube furnace (ThermoScientific, Ashville, North Carolina). The products of the process were then passed through another pressure gauge, a cooling trap and then a back pressure regulator (H. Lorimer Corp., Longview, Texas). While the uncondensed gases exited to be analyzed every hour, the liquid hydrocarbon products were condensed in a condenser maintained at the pressure of the system by the back pressure regulator.

4.2 Experimental Method

4.2.1 Catalyst selection

The conventional Fischer-Tropsch catalyst for the hydrogenation of CO was cobalt supported on silica. The water of the WGS reaction tends to react with the active Fe metal resulting in the formation of the metal oxides. The net result is a reduction in overall conversion and the undesirable increase in methane selectivity. Unlike iron, cobalt catalyst is more resistant to deactivation by the water gas shift reaction (Eq.4.1). Also, cobalt catalysts tend to produce more higher molecular weight hydrocarbons [29,31, 33].

$$CO + H_2O \longrightarrow CO_2 + H_2 \qquad \text{4.1}$$

Generally speaking, supports are expected to disperse the active phase, resulting in an increase in the available metal surface area of the catalyst. Supports stabilize the active phase thereby minimizing loss of active surface area and maintain overall catalyst thermal and mechanical strengths. Support pores and matrix provide a medium for mass and heat transfers for catalysts subjected to diffusion limitations. Catalyst-support interactions can facilitate or inhibit the reduction of the precursors to their active form [33]. Too high an interaction can inhibit reduction, while a loosely bound precursor on the support can lead to catalyst loss to attrition. The nano-particles under those scenarios eventually sinter and agglomerate leading to deactivation. SiO_2 was selected because its

interaction with the metal is small enough to promote reduction but high enough to limit sintering and agglomeration. Metal-support interactions have been shown to decrease in the order Al_2O_3>TiO_2>SiO_2 for the acidic base metal supports [49]. Selection of SiO_2 therefore minimized high support-metal interaction, thereby decreasing the chance for the formation of irreducible forms of cobalt oxide. Such mixed oxides eventually sinter and agglomerate leading to catalyst deactivation [32,39].

The second catalyst supported platinum, palladium and molybdenum on an acid form of ZSM-5 (HZSM-5). Palladium has been reported to have a stabilizing effect by binding active metals to the support although it also plays a key role in reforming/secondary reactions such as isomerization and cyclization [40-41]. Platinum and molybdenum have strong dehydrogenation/hydrogenation capabilities with molybdenum being able to further hydrogenate carbon monoxide, thereby increasing CO conversion [42]. Both metals also have strong metal functionalities in oligomerization and/or polymerization of olefins formed by the conventional catalyst. Platinum also catalyzes the dehydrogenation of alkanes to alkenes in the metal-acid dehydrogenation/hydrogenation reactions involving metal and acidic sites of HZSM-5 [43].

The three metals (Mo, Pd and Pt) are to be supported on a pre-protonated(acid form) of ZSM-5 synthetic zeolite (with Na^+ as the exchangeable cation) with a medium pore size in the range of 5.6-6.0 Å. It has been reported that medium to large pore size ZSM-5 has the effect of facilitating mass transfer within the inter-locking channels [43-44]. The chosen ZSM-5 had a Si/Al ratio of 23. This high acidic property increases the density of the Brönsted acid sites which will only be partially reduced when some of those acid sites are taken up by the three metals introduced in low concentrations. The combination of Co-SiO_2 and Mo-Pd-Pt/HZSM-5 therefore creates a hybrid metal-metal-acid functionalization of the catalyst versus the metal-acid functionality reported in the literature. Hydrocarbons with increased selectivity to jetfuels and diesel can therefore be produced (under appropriate thermodynamic conditions) from an improved Fischer-Tropsch synthesis reaction according to Eq. 4.2 and Eq.4.3:

$nCO + 2nH_2 \longrightarrow C_nH_{2n} + nH_2O$……..……..4.2

$nCO + (2n+1)H_2 \longrightarrow C_nH_{2n+2} + nH_2O$ ……..…..……4.3

The hypothesis is that a hybrid (a mixture of Co-SiO_2 and Mo-Pd-Pt-HZSM-5) catalyst can increase the selectivity of hydrocarbons in the JP-8 and diesel carbon number range versus normal Co-SiO_2 at lower temperatures and pressures in a fixed bed reactor mode of operation.

4.2.2 Catalyst preparation

The silica support was supplied by The Research and Development Center of the PQ Corporation (Conshohocken, Pennsylvania). The cobalt nitrate [$Co(NO_3)_2.6H_2O$] precursor salt was supplied by VWR (Radnor, Pennsylvania). By wet impregnation method, the final catalyst (Co-SiO_2) was prepared to contain 20 wt % cobalt nano-particles. Mass balance calculations showed a total catalyst weight of 25 g for an initial support mass of 20 g. Stoichiometrically, a total of 24.7 g of the nitrate precursor was needed to impregnate 5.0 g of cobalt nano-metals on the support. The calculated weights of the support and salt were then mixed and dissolved in 200 mL of distilled water. For cation adsorption on the support, the equilibrium (Eq.4.4), controlled largely by the pK_a of the acidic surface is established:

$M\text{-}OH^+ + C^+ \leftrightarrow M\text{-}OC^+ + H^+$……..……..4.4

The pH of the metal precursor/silica support solution was raised to 5.4 (with 1.0 N NaOH solution) which is above the point of zero charge (isoelectric point) for the support, reported to be between 1.0-2.3 [31]. Above this pH, the support surface is negatively charged, thereby creating a migration of cobalt precursors to be adsorbed on the SiO_2 surface [31]. The solution was magnetically stirred with simultaneous heating at a temperature between 70 -90 ^oC for at least 18 hours until “dry” to the touch. The “dry” catalyst was then dried in air at a feeding rate of 400 mL/min at 120 ^oC overnight (12 hours) at 1 atm/15 psig. To calcine the catalyst in-situ, the air flow rate was ramped to

500 mL/min and maintained there for 4 hours at a temperature of 400 ^{o}C. Gravimetric measurements showed the difference between the weight of the catalyst and the initial weight of the support to be ~4.6 g, which was approximately the weight of cobalt transferred to the support.

The zeolite was supplied by Zeolyst International (Kansas City, Kansas) and was received in the ammonium form. Since it has been reported that heating in air converts the ammonium to the acid/protonated form [30, 45], the zeolite was converted to the acid form (HZSM-5)] by calcining the ammonium form in 500 mL/min of air at 500 ^{o}C for 4 hours and then cooled. 17.2 g of the support was thus calcined in 500 mL/min of air at 500 ^{o}C for 4 hours and allowed to cool. 14.4 g of HZSM-5 was recovered after removal of nitrogen (as ammonia) and water of hydration. The Mo-Pd-Pt-HZSM-5 catalyst was then prepared by ion-exchange method.

Bis[ethylenediamine]platinum (II) chloride, ammonium molybdate (VII) tetrahydrate-99+% (both powders) and palladium (II) chloride stock solution were precursors for platinum, molybdenum and palladium respectively. Ammonium molybdate (VII) tetrahydrate was supplied by Fischer Scientific (Pittsburgh, Pennsylvania), while the platinum and palladium precursors were both supplied by VWR(Radnor, Pennsylvania). The Mo-Pd-Pt/HZSM-5 catalyst was prepared to contain 8.0 wt % Mo, 1.8 wt % Pd and 1.5 wt % Pt respectively by ion-exchange method. This corresponded to ~1.31 g Mo, 0.2997 g Pd and 0.25255 g of Pt for a total metal loading of 1.862 g. The equivalent amounts of precursors containing these amounts of metals were weighed out after stoichiometric calculations.

The measured amount of bis[ethylenediamine]platinum (II) chloride was dissolved in a predetermined volume of a stock solution of $PdCl_2$ (containing the stoichiometric amount of Pd) and made to 50 mL using distilled water. The predetermined amount of ammonium molybdate (VII) tetrahydrate was completely dissolved in 50 mL of distilled water. This ammonium (VII) tetrahydrate solution was then added to the solution containing bis[ethylenenediamine]platinum (II) chloride and palladium (II) chloride. The combined solution was made to about 250 mL and stirred

continuously to dissolution. The final pH was then adjusted to between 5 and 5.4(using 1.0 N NaOH) since the isoelectric point of ZSM-5 is between 3.0 and 4[46]. The combined precursor mixture was heated (with magnetic stirring) at between 70-90 ^{o}C for at least 20 hours with the HZSM-5 for ion-exchange and then drying to occur. The "dry" catalyst was then oven-dried for 3 hours before being transferred to a micro-reactor where a stream of air at 200 mL/min was passed through it at 110^{o}C for 4 hours. It was then calcined in air at atmospheric pressure at a feeding rate of 500 mL/min for 5 hours at a temperature of 500 ^{o}C. The mass of catalyst at the end of the preparation was ~ 16.1 g. The difference being the weight (combined) of the metals loaded.

4.2.3 Initial reactor startup and catalyst testing

The prepared catalysts Co-SiO_2 and Mo-Pd-Pt-ZSM-5 were ground and sieved to 32-38 μm. Then a total of 1.75 g (1 g of Co-SiO_2 and 0.75 g of Mo-Pd-Pt-ZSM-5) were thoroughly mixed and loaded into a 1.3 cm internal diameter stainless steel micro-reactor supplied by Swagelok (Houston, Texas). 1.0 g of Co-SiO_2 was used in pure Co-SiO_2 experiments. This gave a catalyst bed length of about 40 mm with no pressure drop in the bed. The catalyst bed was trapped between quartz wools. Disks of stainless steel screens (on each side of the bed) delicately welded to stainless steel wires in turn held the wools in place. Before each experiment, the catalyst was activated or reduced in a stream of hydrogen fed at the rate of 150 mL/minute for 12 hours at 400 ^{o}C and 1 atm/15 psig.

With continuous hydrogen flow, the reactor temperature was reduced to 180 ^{o}C at a rate of 1 ^{o}C/minute. Then hydrogen flow was turned off and syngas (H_2:CO ratio of 1.81) was fed into the reactor at 500 mL/minute for 20 minute to purge out residual hydrogen from the catalyst reduction step at 1 atm/15 psig and acclimatize the catalyst for subsequent experiment. It should be noted that the H_2: CO ratio of 1.81 is an adjustment of the maximum syngas composition that would normally be obtained after pyrolysis of sludge from the MixAlco process. This external adjustment is achievable if

the high amount of methane (~20 v%) produced from the pyrolysis of MixAlco process sludge is converted into more hydrogen and carbon monoxide by steam reforming.

This composition is best for the catalytic performance of low temperature (<300 ^{o}C) cobalt catalysts. While maintaining the temperature at 180 ^{o}C the reactor was pressurized gradually with the feed syngas to the two pressures studied: 10 atm/150 psig and 13.6 atm/200 psig maintained using the backpressure regulator. The syngas feed rate was then adjusted to 110 mL/min and the temperature ramped to 250 ^{o}C at a ramp rate of 5 ^{o}C /min. For each set of conditions, the experiments were performed in duplicate. It should be noted that multiple preliminary experiments at 300 and 320 ^{o}C and at a pressure of 20 atm/300 psig were attempted. Since these experiments gave very high conversions, but couldn't yield any meaningful liquid hydrocarbons due to diffusion limitations, only the conditions 10 atm/150 psig and 13.6 atm/200 psig at 250 ^{o}C were investigated. A residence time (inverse gas hour space velocity) of 269 gmin/mol was used and calculated using Equations 4.5-4.7. Table 4.1 summarizes the key catalyst reduction and operating reactor parameters and conditions.The feeding rate of 110 mL/minute was maintained at the inlet for a time on stream (TOS) of 9 hours.

$$\frac{W_{cat}}{feed_{ideal\ gas}} = \frac{W_{cat}}{\dot{n}_{ideal\ gas}} = \text{inverse GHSV} = \frac{RTW_{cat}}{p_{ideal\ gas} \times \dot{Q}} \quad \text{.....4.5}$$

$$\dot{n}_{ideal\ gas} = \frac{p_{ideal\ gas} \times \dot{Q}}{RT} \quad \text{.....4.6}$$

$$p_{ideal\ gas} = \text{species mole fraction} \times P^{*} \quad \text{.....4.7}$$

Table 4.1 Catalyst reduction and experimental operating parameters and conditions

reduction in hydrogen					
temperature(^{o}C)	pressure (atm)	H_2 flow (SLPM)	H_2 flow (kmol/min)	time(hours)	W/F (gmin/mol)
400	1	150	6.1	12	187
experimental run					
temperature(^{o}C)	pressure (atm)	syngas flow (SLPM)	syngas flow (kmol/min)	time (hours)	W/F (gmin/mol)
250	10, 13.6	110	4.5	9	269

4.2.4 Analysis

Uncondensed effluent gas samples were collected every hour for analysis using 0.5 L tedlar bags supplied by SKC Inc. (Houston, Texas) following the attainment of the predetermined thermodynamic conditions of temperature and pressure at reactor startup. The uncondensed regular gases namely unconverted CO and CO_2 were analyzed using an SRI 8610C GC equipped with an HID and a TCD detector. The SRI GC sampling loop was programmed to inject 1.0 mL of gas sample per injection. The uncondensed C_1-C_6 hydrocarbons were analyzed using another SRI 8610C GC equipped with a 30 m×0.53 mm×40 μm HP-plot/Q column supplied by Agilent Technologies (Santa Clara, California). 20 μL of gas sample was injected using a gas-tight syringe. The condensed hydrocarbons were collected at the end of the TOS and analyzed using a GCMS (Thermo Electron Corporation, Pittsburgh, Pennsylvania) having an Rxi 5ms 60 m×0.25 mm×0.25 μm column.

The SRI GC was previously calibrated with lower olefin (alkene) and paraffin (alkane) (C_2-C_6) standards including methane. The quantification of the concentration of each of the lower/lighter hydrocarbon product was therefore based on a calibration one-point coefficient after the injection of 20 μL of sample. Calibration coefficients are shown in Table A 3 in the Appendix section. After collection of the liquid product, it was allowed to settle for the establishment of a phase separation of the top lighter hydrocarbons from the bottom water phase.

A liquid-tight glass syringe was used to withdraw 100 μL of the top hydrocarbons part. This was then transferred into a 100 μL insert vial contained in a 2 mL GCMS sampling vial. 0.5 μL of the liquid hydrocarbons product was injected into the GCMS by the auto-sampler undiluted using a 250:1 split ratio with a split flow rate of 375 mL/minute. The GC initial temperature was 50 ^{o}C and was maintained there for 5 minutes before ramping to 320 ^{o}C at a ramp rate of 20 ^{o}C/minute. The temperature was maintained at 320 ^{o}C for 5 minutes. The helium carrier gas flow rate was 1.5 mL/min with an inlet temperature of 225 ^{o}C. The MS ion source and transfer line temperatures were maintained at 250 ^{o}C. The analysis of only the top portion of the liquid sample following a phase separation ensured that the injected samples were purely hydrocarbons in composition with negligible amounts of oxygenates if ever produced. Target compound spectra (fingerprints) generated in GCMS chromatogram were matched with the spectra of candidate compounds suggested from the library established by the NIST.

The effluent and feed CO concentrations were used to establish the % conversion (X) as defined in Equation 4.8. Since over 130 hydrocarbons were detected and identified, a semi-quantitative method based on the peak areas of the compounds was used to determine the selectivity of hydrocarbons within a given carbon number range in the effluent stream. The sum of the peak areas of hydrocarbons with a given carbon number in the effluent stream was first calculated. The selectivity of all hydrocarbons within that carbon number range was then obtained by expressing the sum of their peak areas as a percentage of the difference between the sum of the peak areas of all hydrocarbons and the sum of the peak areas of the hydrocarbons in that carbon number

range. See Equation 4.9. Because of the sampling method, the gas phase (CO, CO_2 and C_1-C_6) and liquid phase analyses were performed separately. The compositions of CH_4 and CO_2 were plotted against the TOS. The selectivities of C_2 to C_6 were determined (based on effluent concentrations) at steady state conversion when catalyst deactivation was minimal, or at the peak of limiting reagent conversion in the case where deactivation was observed.

$$\% \text{ CO conversion (X)} = \frac{\text{CO feed concentration} - \text{CO exit concentration}}{\text{CO feed concentration}} \times 100 \quad \ldots\ldots 4.8$$

$$\text{selectivity, wt\%} = \frac{\sum_{i=p}^{q} A_i}{\sum_{i=6}^{n} A_i - \sum_{i=p}^{q} A_i} \times 100,\ p < q < n \quad \ldots\ldots 4.9$$

The distributions of the various classes of hydrocarbons (paraffins, olefins and isomers) were determined by expressing the sum of the GCMS peak areas of the hydrocarbons in each class as a percentage of the total hydrocarbons peak area. The two-sample t-test was used to statistically compare the selectivities (from the cross-over points of the selectivity versus carbon number plots) of the two catalysts; Co-SiO_2 and Co-SiO_2/Mo-Pd-Pt-HZSM-5 at 10 atm/150 psig at 250 ^oC using Minitab 16 statistical environment. The same statistical technique was used to compare the selectivities of the hybrid catalyst at two pressures 10 and 13.6 atm at 250 ^oC. In each case, after the cross-over point in the selectivity versus carbon number plot, the mean selectivity of the hydrocarbons with carbon numbers of 12 or more were compared. This method was used because the area under the selectivity versus carbon number plot has no real physical significance.

4.2.5 Characterization

Specific surface area characterizations of the supports and then the catalysts were performed using a multi-point BET surface area analyzer with nitrogen as the adsorbate

in a Nova 4200e supplied by Quantachrome Instruments (Boynton Beach, Florida). Samples were first pretreated by vacuum degassing for a period of 3 hours at 320 ^{o}C. The pretreated samples were then transferred to the analysis station at an adsorbate temperature of -195 ^{o}C. Nitrogen was delivered into the sampling cells for a period of 1 hour. The specific surface area of the ZSM-5 dropped from 559 m^2/g to 120.9 m^2/g after loading with Mo, Pd and Pt in Mo-Pd-Pt/HZSM-5. When the SiO_2 was loaded with Co, its specific surface area dropped from279.9 m^2/g to 118.3 m^2/g. The determined specific surface area of the acid form of ZSM-5, HZSM-5 was 230.6 m^2/g.

Electron probe microanalysis (EPMA) was used to qualitatively verify the presence of each metal on the support. Backscattered electron images (BSE) and elemental analyses were acquired on a four wavelength-dispersive spectrometer (WDS) Cameca SX50 electron microprobe at an accelerating voltage of 15 kV and beam currents of 1 to 100 nA. Energy-dispersive X-ray (EDS) qualitative analyses (spectra) were obtained with the SX50's Imix Princeton Gamma Tech (PGT) system using an ultra-thin window detector. Wavelength-dispersive X-ray (EDS) qualitative scans (spectra) for Pd and Pt were obtained with the SX50's PET diffracting crystals at an accelerating voltage of 15 kV and a beam current of 100 nA. X-ray elemental distribution "maps" were obtained with wavelength dispersive spectrometers (WDS) at 15 kV and 20 nA beam current in beam scanning mode. The beam was rastered in either a 128 by 128 point grid with a grid spacing of 0.07 micron (10,000x mag), or a 256 by 128 grid with a grid spacing of 0.24 micron (1500x mag). The X-ray acquisition time per grid point (pixel) was 15 milliseconds. The inverted x-ray maps for cobalt on silica and for molybdenum, palladium and platinum on HZSM-5 are shown in Figure 4.2.

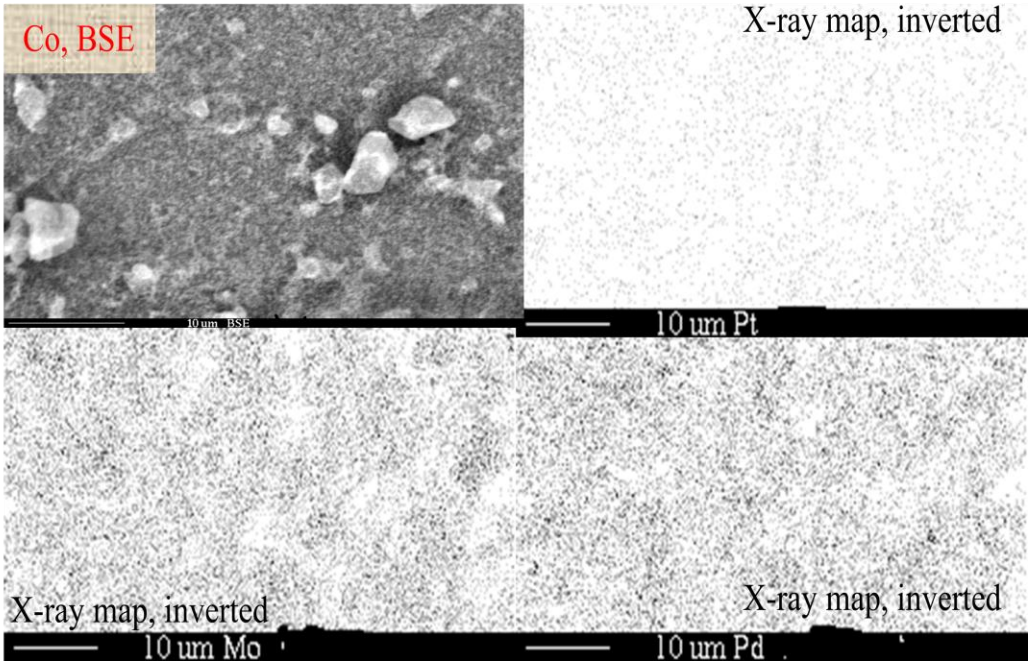

Figure 4.2 BSE for Co (top left) and x-ray images for Mo (bottom left), Pd (bottom right) and Pt (top right)

Preliminary characterization entailed determining actual x-ray counts for the elements of cobalt, molybdenum, palladium and platinum on their respective supports. Because of relatively higher concentrations of cobalt and molybdenum, EDS x-rays of these two elements were easily discernible from the x-ray spectra. The lower concentrations of palladium and platinum made their own spectra peaks relatively weak. The dark images in Figure 4.2 indicate the locations of the respective metals. Inverted x-ray maps of the pure supports when compared to the actual catalysts showed relatively reduced visual appearances of dark images due largely to the presence of exchangeable sodium cations for the zeolite support. To ascertain the presence these two metals, a WDS scan was performed and the peaks for detected palladium and platinum are shown in Figure 4.3.

Four candidate catalyst grains were examined for the distribution of the metals. The cobalt dispersion was relatively dense owing to the high loading with clusters

unevenly spread on the support matrix. From the backscattered electron and the x-ray maps, the relative surface presence of the metals were Co> Mo>Pd>Pt. The presence of clusters was common to both catalysts probably pointing to localized regions of metal nano-particle sintering and agglomerization especially as a significant surface of the catalyst showed evidence of uniform distribution. Reduction in sintering and agglomerization was probably aided by magnetic stirring during aging and longer periods of drying in air.

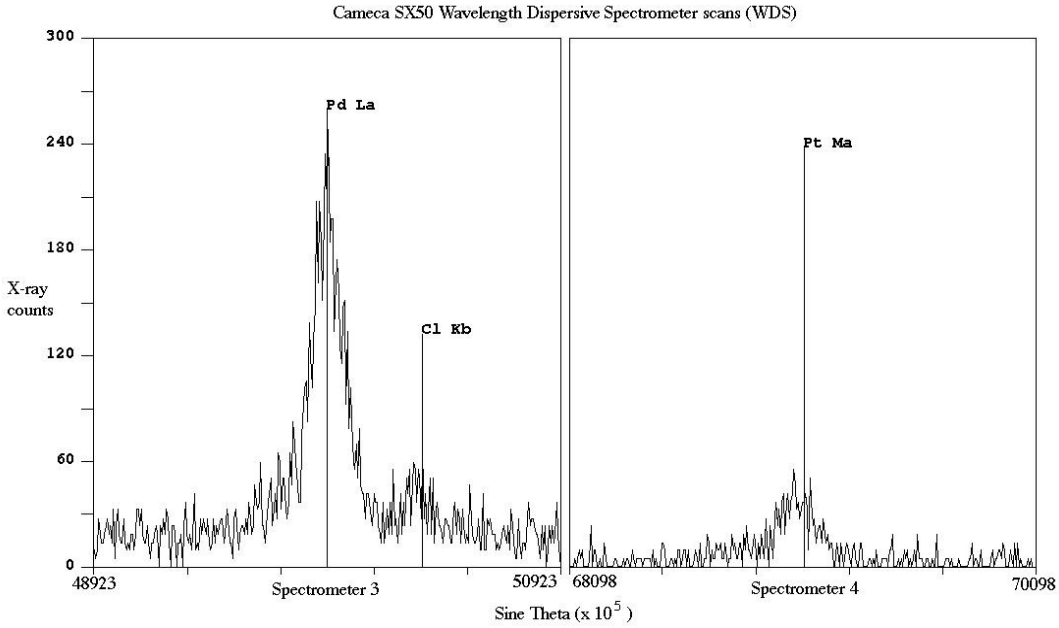

Figure 4.3 Results of WDS scans for palladium and platinum

4.3 Results and Discussion

4.3.1 Co-SiO_2 versus Co-SiO_2 /Mo-Pd-Pt-HZSM-5 catalyst (250 ^oC and 10 atm)

About 123 to 130 hydrocarbon compounds were identified for the Co-SiO_2 catalyst while 135 to 148 hydrocarbon compounds were identified when the hybrid catalyst was used. The hydrocarbons were in the classes of striaght-chained n-alkanes/paraffins, alkenes/olefins and isomers with isomers being mono-, di-, tri- and tetra-branched.

The usual Co-SiO_2 catalyst produced hydrocarbons primarily in the gasoline (C_4-C_{12}) carbon number range at 250 ^oC and 10 atm. The gasoline fraction had its highest selectivities in the C_9 to C_{11} carbon number range with lower selectivities of JP-8 (C_{10}-C_{17}). Under a similar condition, and using Co-SiO_2/Mo-Pd-Pt-HZSM-5 catalyst, the maximum selectivity reduced (from ~19.8 to ~10) but the selectivity of fuel in the JP-8 carbon number range showed an increase as can be shown by the shift in the selectivity curve of the hybrid catalyst in Figure 4.4. See Figure A 4 and Tables A 5-A 6 respectively in the Appendix for liquid hydrocarbons chromatogram and nomenclature for results at 10 and 13.6 atm for a temperature of 250 ^oC.

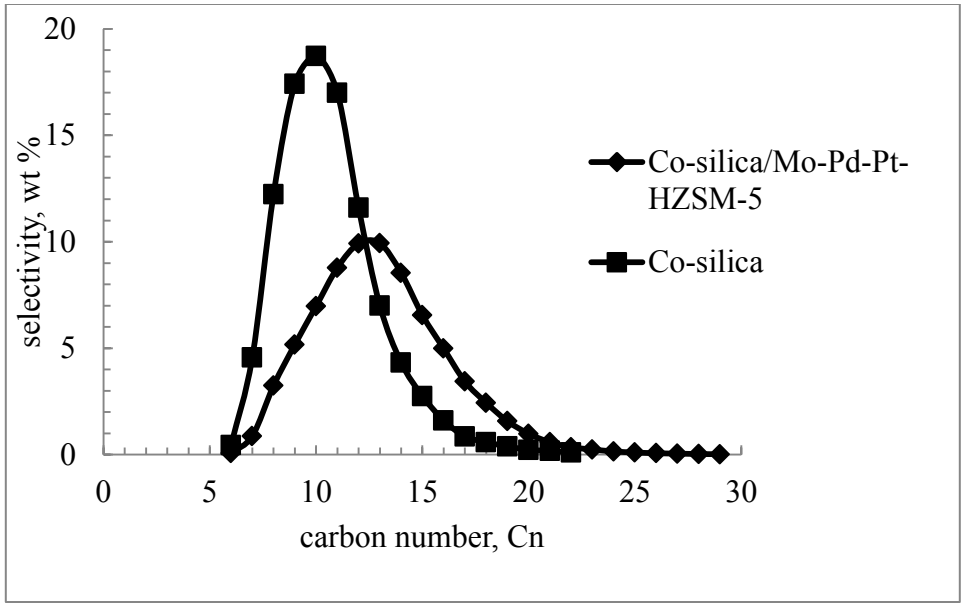

Figure 4.4 Effect of catalyst on hydrocarbons selectivity at 250 ^{o}C and 10 atm

The result shows that mixing Co-SiO_2 catalyst with Mo-Pd-Pt-HZSM-5 can increase the selectivity of the conventional Fischer-Tropsch catalyst to higher hydrocarbons in the JP-8 range. However, Figure 4.5 shows that Co-SiO_2 catalyst will produce more isomer and olefins than the hybrid catalyst. Furthermore, more straight-chained hydrocarbons in the JP-8 range are produced for the Co-SiO_2/Mo-Pd-Pt-HZSM-5 over Co-SiO_2 catalyst. Thermodynamics favors the oligomerization of lower olefins to longer chain hydrocarbons at temperatures lower than 300 ^{o}C (low temperature Fischer-Tropsch processes). Therefore, at 250 ^{o}C lower olefins diffuse through the pores of the Mo-Pd-Pt-HZSM-5 catalyst component to become hydrogenated on the Brönsted acid sites of the Mo-Pd-Pt-HZSM-5 to produce active carbonium ion intermediates. The metal functionalization of the HZSM-5 then leads to the combination of the carbonium ions (during olefins oligomerization) to form longer chain n-paraffins. Hence the increase in the relative amounts of paraffins [44].

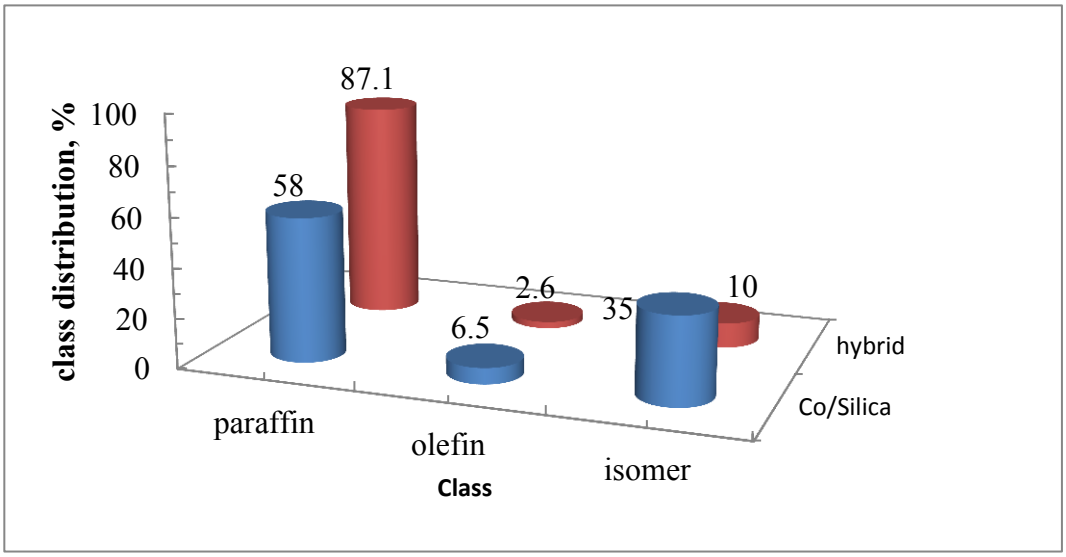

Figure 4.5 Distributions of the various classes of hydrocarbons for the two catalysts at 10 atm and 250 ^{o}C

It would appear that isomerization is favored over oligomerization on Co-SiO_2. Since the olefins are starting materials for active intermediate ions (carbonium ions) needed for secondary reactions, more olefins diffuse through the acidic pores of the Co-SiO_2 where they become chemisorbed and protonated on the acid sites to become tertiary, secondary and primary intermediates. The carbonium ions then diffuse and become isomerized into mono-, di-, and tri-branched isomers [44]. In the Co-SiO_2/M-Pd-Pt-HZSM-5 catalyst, the intermediates from olefin hydrogenation are thermodynamically used as materials for oligmerization to JP-8, rather than for isomerization. When Co-SiO_2 is the catalyst, the intermediates isomerize. This explains an increase in the amount of isomers in the Co-SiO_2 versus the Mo-Pd-Pt-HZSM-5 catalyst. Hence Co-SiO_2 seems to be a good catalyst for the production of predominantly gasoline fuels. Mixing Co-SiO_2 with Mo-Pd-Pt-HZSM-5, therefore creates a hybrid catalyst for the production of fuels predominantly in the JP-8 boiling range. Although there might be a decrease in the octane rating, due to decrease in the distribution of

isomers or olefins, the overall power output increases because of the increase in the molecular weights of the species hydrocarbons. No aromatics were produced largely due to thermodynamic reasons.

4.3.2 Hybrid catalyst –conversion and CO_2 and CH_4 productions at 10 and 13.6 atm and 250 ^oC

Figure 4.6 shows the carbon monoxide conversion vs the time on stream for the hybrid catalyst at 250 ^oC studied for two pressures; 10 and 13.6 atm. After a brief transient period for both conditions, conversion of CO quickly peaked at around 88 %. Steady state performance was maintained at the condition of 13.6 atm, while deactivation of the catalyst was observed after 5 hours for the condition of 10 atm. It has been reported in the literature that condensation of gas phase hydrocarbons on the catalyst surface leads to deactivation through carbon nano-rods formation on the surface of the catalyst [47].

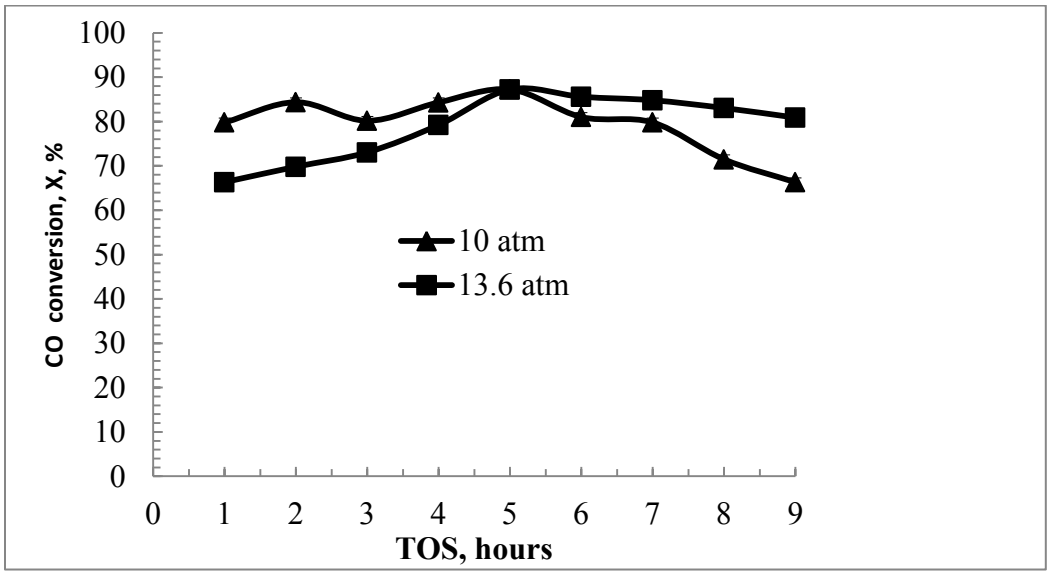

Figure 4.6 Conversion vs time on stream for the hybrid catalyst at 10 and 13.6 atm (250 ^oC)

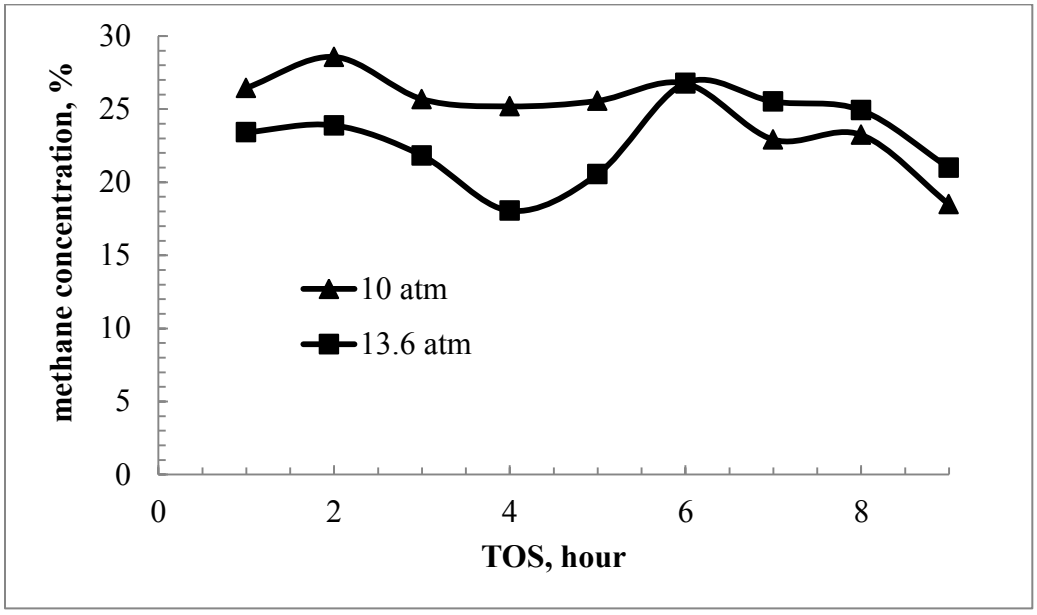

Figure 4.7 Variations in the CH_4 concentrations at 10 and 13.6 atm

Figure 4.7 shows how the methane concentration in the effluent changed with the time on stream for the two pressures. The change with the time on stream (TOS) of the concentration of carbon dioxide is shown in Figure 4.8. At a high catalytic activity which corresponded to steady state CO conversion, the product stream concentration of ethylene seemed low compared to when deactivation kicked in. The corresponding methane concentrations seemed to be highest. This suggested ethylene cleavage into methane. The latter being a stable molecule is unlikely to undergo carbon-carbon coupling secondary reactions into higher hydrocarbons. Whence, methane partial pressure and its concentration in the effluent gas phase will be expected to increase.

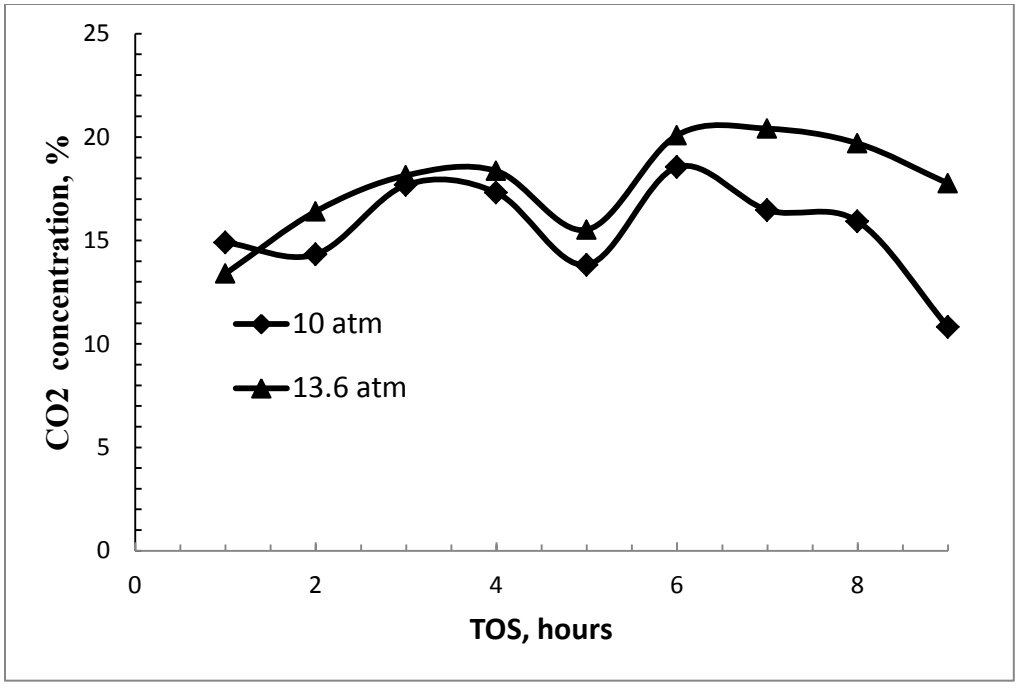

Figure 4.8 Variations in the CO_2 concentrations at 10 and 13.6 atm

The difference in methane concentration at the two pressures is best explained by the Anderson-Schulz-Flory (ASF) statistical model. At lower pressures, the probability for chain growth (α) in the propagation step of the overall reaction decreases so that more short chain hydrocarbons (C_1-C_3) are produced. In particular methane will have the highest selectivity. As the pressure increases the value of α also increases. This then increases the selectivity of higher hydrocarbons leading to a decrease in the selectivity of methane.

The increase in the selectivity of CO_2 at higher pressures is best explained partly by the stoichiometry of the water gas shift reaction and the overall reaction kinetics during the transient state of the reaction. An extra mole of CO_2 is produced for an additional mole of CO consumed at a higher pressure. At higher pressures, the concentration of CO in the gas phase (and hence its number of moles converted)

increases. This means that the rate of steam reforming of the extra CO to produce more CO_2 in the forward WGS reaction will increase. The reverse occurs at lower pressures when the concentration of CO reduces at a lower CO catalyst bed pressure leading to a reduction in the concentration of the CO_2 in the effluent. Since an explicit kinetics study of the WGS reaction was not the main objective of this work, one can only speculate an increase in the rate of the forward reaction producing more CO_2 product species at higher catalyst bed pressures, with the reverse occurring at lower pressures [53].

4.3.3 Hybrid catalyst – uncondensables at 10 and 13.6 atm (250 ^{o}C)

The plot of selectivities at 10 and 13.6 atm for a temperature of 250 ^{o}C is shown in Figure 4.9 for C_1 to C_6 hydrocarbons. The distributions of the various hydrocarbons classes are shown in Figure 4.10 for the same non-condensables (C_1 to C_6). At higher pressures, there is a general drop in the selectivity of the lower hydrocarbons compared to the selectivity at lower pressures. Since it was also observed that an increase in pressure caused an increase in the selectivity of higher hydrocarbons in the JP-8 and diesel range, increase in pressure probably favored more secondary oligomerization reactions of the lower hydrocarbons to higher hydrocarbons. For the non-condensable hydrocarbons, the selectivity also decreases with the carbon number for all two pressures studied. Lower hydrocarbons, especially (C_2-C_4) olefins are some of the main products of the primary Fischer-Tropsch synthesis process [40]. At a low probability for the propagation of the active intermediates (usually at low reactor pressures), the selectivity of lower hydrocarbons will be expected to increase.

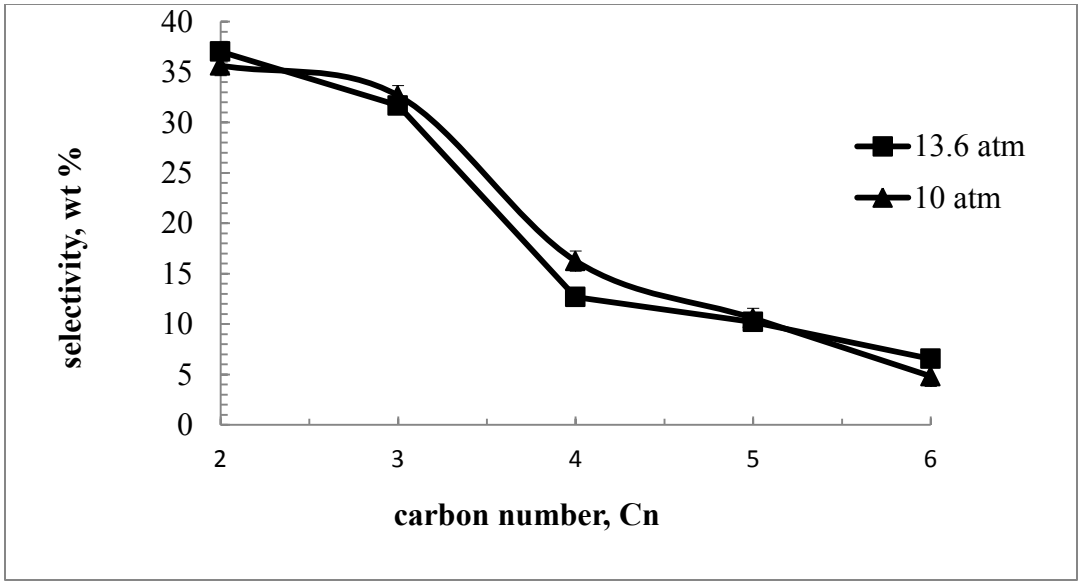

Figure 4.9 Selectivity versus the carbon number for uncondensables

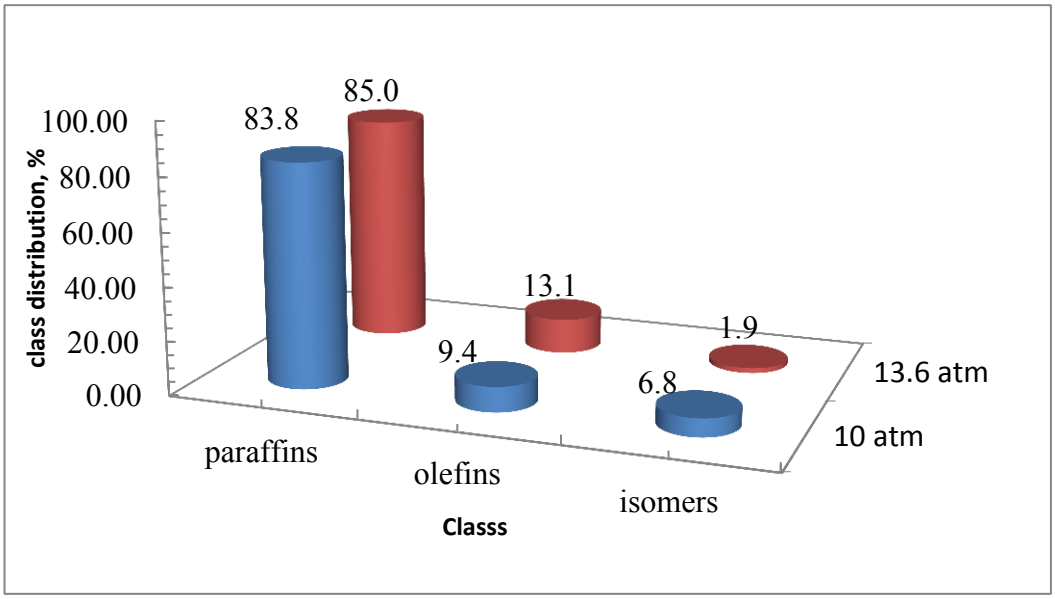

Figure 4.10 Class distributions for the uncondensables

At both 10 and 13.6 atm, results show the production of lower paraffins, lower olefins and lower isomers. Increasing the pressure from 10 to 13.6 atm causes an increase in the amount of n-paraffins, an increase in the amount of olefins and a decrease in the amount of isomers. An increase in the pressure increases the concentration of CO in the gas phase. This increases the production of lower olefins which become protonated by the Brönsted acid sites of the Mo-Pd-Pt/HZSM-5 catalyst and the acidity of the SiO_2 to increase the concentration of carbonium ions ions. The intermediates then oligomerize on the metal sites to produce shorter chain n-paraffins. Thermodynamics still favors oligomerization over isomerization.

4.3.4 Hybrid catalyst – selectivities and class distributions at 13.6 atm (250 ^{o}C)

In order to investigate the influence of pressure on selectivity and product class distribution, runs were carried out for the catalyst Co-SiO_2/Mo-Pd-Pt-HZSM-5 at 13.6 atm and 250 ^{o}C. As shown in Figure 4.11, the selectivities of JP-8 and to some extent diesel automotive fuels increased when the results were juxtaposed with results obtained at 10 atm and 250 ^{o}C.

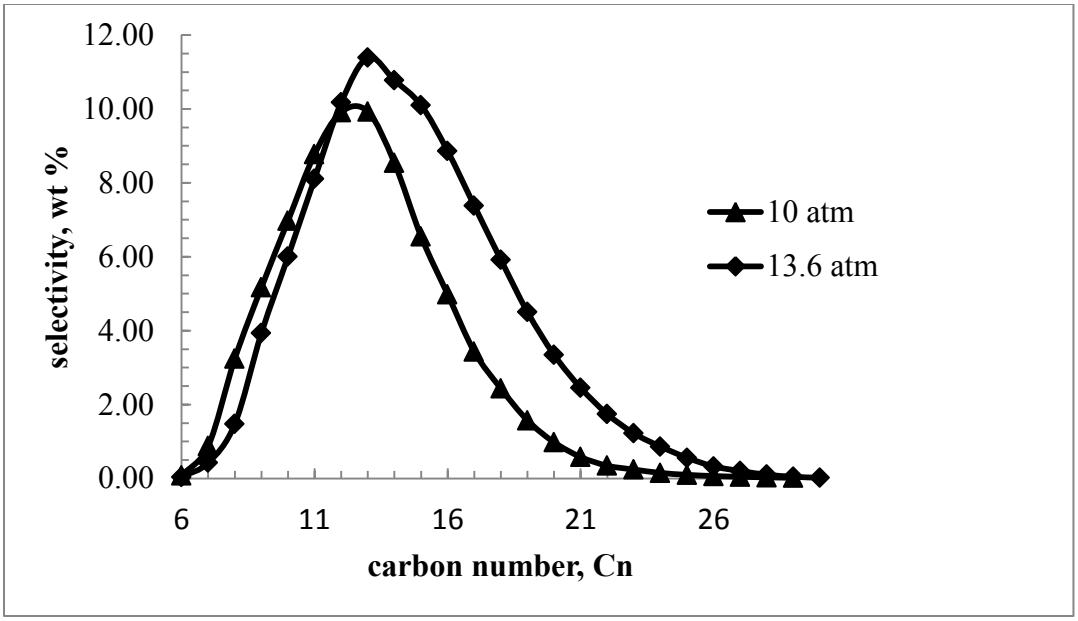

Figure 4. 11 Increase in selectivity with increase in pressure for the Co-SiO_2/Mo-Pd-Pt-HZSM-5 hybrid catalyst

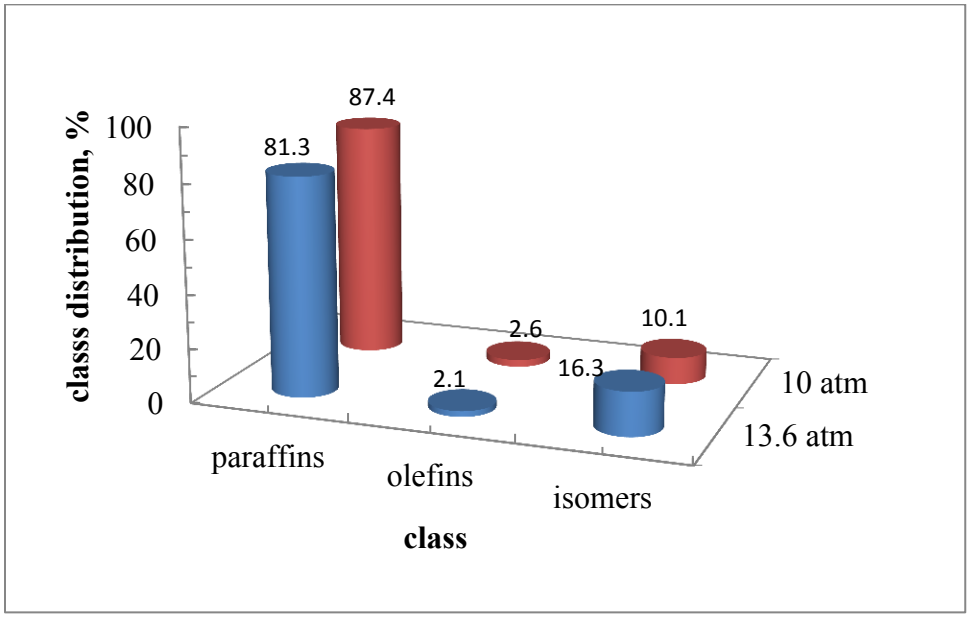

Figure 4.12 Product class distribution for the Co-SiO_2/Mo-Pd-Pt-HZSM-5 hybrid catalyst

From Figure 4.12 this increase is at the expense of paraffins and olefins. At the same time enhanced isomerization of the olefins and a decrease in the paraffin selectivity are observed. At higher pressures, dehydrogenation of the paraffins to the olefins could occur. If the olefins become rehydrogenated on the acid sites of the catalyst, the intermediates produced can in another metal functionality of the catalyst become isomerized into more isomers. Given the low temperature at which the experiments were performed, the likelier scenario is that the olefins already generated from the primary FTS process immediately undergo hydrogenation on the acid sites followed by the metal functionalization of the carbonium ions into isomers. This means that an increase in pressure promotes isomerization at the expense of oligomerization and/or polymerization into straight-chained paraffins. The mean difference in selectivity of the Co-SiO_2/Mo-Pd-Pt-HZSM-5 catalyst over Co-SiO_2 was 0.61 with a p-value of 0.29. The mean difference in selectivity of the Co-SiO_2/Mo-Pd-Pt-HZSM-5 when the pressure was raised to 13.6 atm from 10 atm was 1.53 with a p-value of 0.11. Selectivity of a conventional FTS process could therefore be altered in two ways: changing the catalyst for the same condition and altering process thermodynamics for the same catalyst.

4.3.5 Proposed reaction mechanisms

The 3 main secondary reactions affecting product selectivity are isomerization, oligomerization and polymerization (to long-chain paraffins). All three reactions depend on the products of the Co-SiO_2 primarily olefins and involve the formation of active intermediate carbonium ions. When the selectivity of JP-8 is increased, the major hydrocarbons class distribution shows that the relative amounts of the various classes increase in the order paraffins > isomers> olefins for the hybrid catalyst at both pressures of 10 and 13.6 atm respectively. One might then conclude that at the thermodynamic state of the system, the predominant secondary reactions are oligomerization and/or polymerization followed by isomerization. Free available olefins from primary FTS reaction and to some extend those generated from the metallic dehydrogenation of lower

alkanes are converted to intermediates and those intermediates are in turn preferably converted more to longer-chain hydrocarbons by oligomerization and/or polymerization over isomerization.

Figure 4.13 shows how propane and/or propylene can be polymerized to a longer-chain hydrocarbon (via dehydrogenation into propylene) with the created intermediate possibly undergoing a parallel isomerization reaction. Both reactions feed on a common propylene pool with the propylene generated from the catalytic activity of Co-SiO_2 and from the metal dehydrogenation of propane.

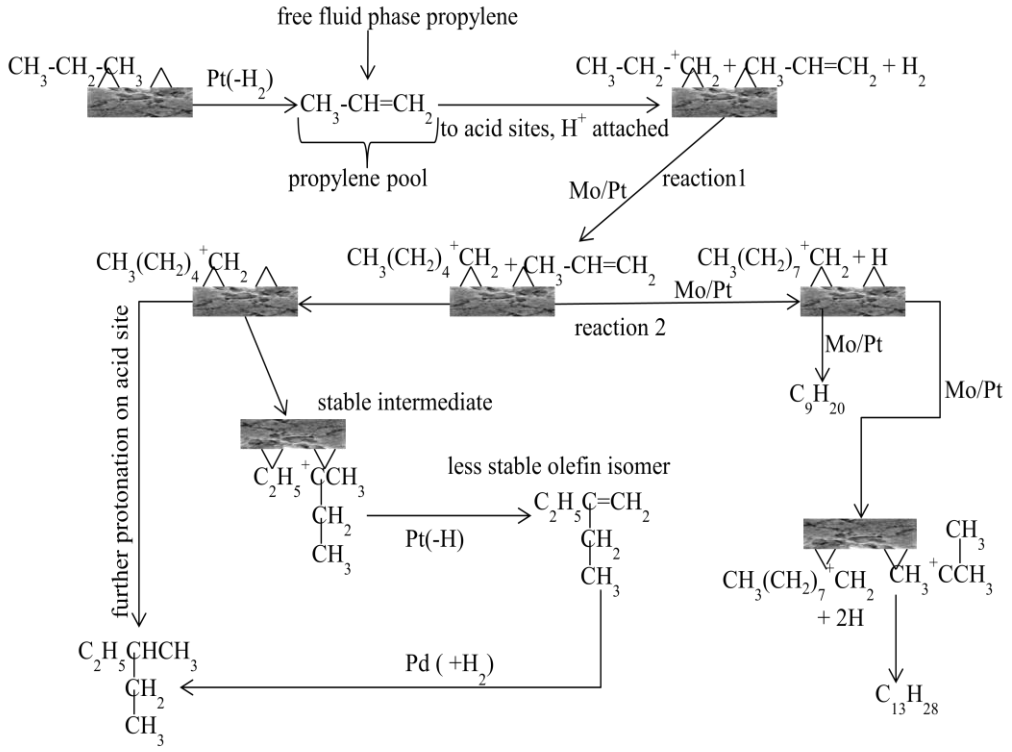

Figure 4.13 Proposed mechanisms for the oligomerization of propylene and the isomerization of the derived intermediates

When the alkanes are used as starting materials for secondary reactions, they are first converted to olefins by the dehydrogenation activity of the platinum on HZSM-5. This is because, alkane adsorption on to ZSM-5 is limited but will chemisorb in the presence of a transition metal to become dehydrogenated to their corresponding alkene or olefins, thereby increasing the olefin pool [44]. With the aid of acid sites and Mo/Pt catalytic activities, propagation to longer chain alkanes will occur with Pd catalyzing the isomerization reactions.

Oligomerization reaction reduces the total number of hydrocarbons in the system, thereby reducing the overall system entropy versus isomerization which leaves the entropy somewhat the same. This leads to a greater negative change in the Gibbs free energy thereby encouraging species propagation over structural reconfiguration as is the case with isomerization. Less isomers are therefore produced. The dehydrogenation of a paraffin to an olefin, the attachment of olefins to free acid sites to generate intermediates and the eventual surface interaction of the intermediates to form the longer chain paraffins are Langmuir-Hinshelwood-Hougen-Watson style mechanistic steps [48]. Since the possibility also exists for the interaction of a surface adsorbed intermediate with a free fluid phase olefin to form a JP-8 molecule in a final step, the Eley-Rideal mechanism also comes into play.

4.4 Chapter Summary

Experiments were performed to catalytically convert syngas with the composition of 65 mol % H_2 and 35 mol % CO using a conventional Fischer-Tropsch synthesis catalyst (Co-SiO_2) at a pressure of 10 atm and a temperature of 250 ^oC. The liquid product obtained contained hydrocarbons mainly in the gasoline and JP-8 carbon number ranges.

When this catalyst was mixed with a newly designed Mo-Pd-Pt/HZSM-5 catalyst with a metal-metal-acid functionality, the resulting hybrid catalyst caused the selectivity of the liquid product to shift more to the hydrocarbons in JP-8 carbon number range. At a higher pressure of 13.6 atm and a temperature of 250 ^oC, the selectivity of

hydrocarbons with their carbon numbers within the JP-8 and to some extent diesel was further increased. Hence using the hybrid catalyst and the MixAlco process derived syngas with the stated composition will enable the process extend its fuels production to more JP-8, gasoline and diesel. This will go a long way to increase the fuels production capacity of the plant.

CHAPTER V
CONCLUSIONS

5.1 Syngas from the Pyrolysis of MixAlco Process Sludge

Under the conditions at which the pyrolysis of the feed was conducted, it was found that the undigested effluents from the MixAlco process can be pyrolyzed to recover hydrogen, carbon monoxide (as the major components of synthesis gas) together with methane. The key pyrolysis findings can be summarized as follows:

1. operating at 630-770 ^{o}C with a biomass feed rate of 300-400 g/minute, an auger pyrolyzer and the response surface statistical method were use to obtain a maximum syngas composition of 43.9±3.36 v % H_2/33.3±3.29 v % CO at 740 ^{o}C. The CH_4 concentration was 20.3±2.99 v %. It was projected that, up to 5,990 g H_2 (719.3MJ), 65,000 g CO (660 MJ) and 21,170 g CH_4 (1,055.4 MJ) can be produced at optimum condition per ton of sludge pyrolyzed. At optimum composition a ton of pretreated sludge produced up to 5,990 g of internal hydrogen for the hydrogenation of ketones to a mixture of alcohols in the MixAlco process. This reduces their projected price per gallon of fuels produced by this process from US $1.24 to US $1.00 making the process more competitive.

2. the energy efficiency decreases with increase in temperature, the process also being energy neutral. The energy neutrality of the process can be further enhanced by recycling up to 1,715.4 MJ of energy from the combustion of CO and CH_4 combined(per ton of sludge pyrolyzed) when the process is operated under optimum conditions.

5.2 Hydrogen Separation by PSA

Pressure swing adsorption can be used to recover hydrogen efficiently from the syngas derived from the pyrolysis of sludge from the MixAlco process, although such syngas sources traditionally have lower concentrations of hydrogen versus industrial

sources. Under the condition at which PSA hydrogen separation was performed it can be concluded that:

1. An increase in the percent cycle recovery with increase in the amount of adsorbent used does not always translate into an increase in cycle bed productivity with a 99.9 % H_2 purity achieved. In particular, after maximum cycle bed productivity is reached, further increase in % recovery only leads to a decrease in cycle bed productivity. At a maximum CBP of 66.2 % up to 3,965.4 g of hydrogen will be recovered from the PSA unit per ton of pretreated sludge pyrolyzed.

5.3 Production of Liquid Transportation Fuels from Syngas

A low temperature cobalt based enhanced Fischer-Tropsch synthesis catalyst with a metal-metal-acid functionality (Co-SiO_2/Mo-Pd-Pt-HZSM-5) can be used to produce liquid transportations in an add-on catalytic process to the MixAlco process using syngas derived from the pyrolysis of the MixAlco process sludge. This boosts its overall fuel production capacity since the gasoline (C_4-C_{12}), JP-8(C_{10}-C_{17}), diesel (C_{16}-C_{25}) were produced. Within the range of our experimental conditions we conclude as follows:

1. At 10 atm and 250 ^oC, Co-SiO_2/Mo-Pd-Pt-HZSM-5 hybrid Fischer-Tropsch catalyst can be used to increase the selectivity of JP-8 versus Co-SiO_2 conventional catalysts in a fixed bed continuous flow system.

2. Raising the pressure to 13.6 atm, the Co-SiO_2/Mo-Pd-Pt-HZSM-5 catalyst will further increase the selectivity of JP-8 and to some extent diesel automotive fuels at a pressure lower than the 20 atm reported in the literature. The extra production capacity of the process has the potential to make biomass-to-liquid production process plants more competitive in addition to the overall environmental costs savings.

REFERENCES

[1] Pham V, Holtzapple M, El-Halwalgi M. Techno-economic analysis of biomass to fuel conversion via the MixAlco process. J Ind Microbiol Biotechnol 2010;37:1157-1168.

[2] Bao J, Yang G, Okada C, Yoneyama Y, Tsubaki N. H-type zeolite coated iron-based multiple-functional catalyst for the direct synthesis of middle isoparaffins from syngas. Applied Catalysis A:General 2011;394:195-200.

[3] Shetian L, Amit C G, Peter Thomas, Toghiani H, White M. G. Synthesis of gasoline-range hydrocarbons over Mo/HZSM-5 catalyst. Applied Catalysis A : General, 2009;357:18-25.

[4] Xiaohong L, Mengfei L, Kenji A. Direct synthesis of iso-paraffins from synthesis gas on hybrid catalysts. Catalysis Today 2004;89:439-446.

[5] Angenent Largus T. Energy biotechnology: beyond the general lignocellulose-to-ethanol pathway.Current Opinion in Biotechnology 2007;18:191-192.

[6] Keshav T R, Basu S. Gas-to-liquid technologies; India's perspective. Fuel Processing Technology 2007;88:493-500.

[7] Strezov V, Patterson M, Zymla V, Fisher K, Evans T J, Nelson P F. Fundamental aspects of biomass carbonization. J Anal Appl Pyrolysis 2007;79:91-100.

[8] Zhang Q, Chang J, Wang T, Xu Y. Upgrading bio-oil over different solid catalysts. Energy & Fuels 2006;20:2717-2720.

[9] Anh N P, Changkook R, Vida N, Sharifi, Jim S. Characterisation of slow pyrolysis products from segregated wastes for energy production. J Anal Appl Pyrolysis 2008; 81:65-71.

[10] Hossain Mustafa K, Vladimir S, Nelson Peter F. Thermal characterization of the products of wasterwater sludge pyrolysis. J Anal Appl Pyrolysis 2009;85:442-446.

[11] Asadullah M, AnisurRahman M, Mohsin Ali M, Abdul Motin M, Borhanus Sultan M, Robiul Alam M, SahedurRahman M. Jute stick pyrolysis for bio-oil production in fluidized bed reactor. Bioresource Technology 2008;99:44-50.

[12] Graca I, Ramoa Ribeiro F, Cerqueira H S, Lam Y L, de Almeida M.B.B. Catalytic cracking of mixtures of model bio-oil compounds and gasoil, Applied Catalysis B: Environmental 2009;90:556-563.

[13] Botesa F G, Böhringerb W. The addition of HZSM-5 to the Fischer-Tropsch process for improved gasoline production. Applied Catalysis A: General 2004;267(1-2):217-225.

[14] Martíneza A, Valencia S, Murcianoa R, Cerqueirab H S, Costac A F S, Aguiarc E F. Catalytic behavior of hybrid Co/SiO_2-(medium-pore) zeolite catalysts during the one-stage conversion of syngas to gasoline. Applied Catalysis A:General 2008;346(1-2):117-125.

[15] Park H J, Dong J-I, Jeon J-K, Park Y-K, Yoo K-S, Kim S-S, Kim J, Kim S. Effects of operating parameters on the production of bio-oil in the fast pyrolysis of Japanese larch. Chemical Engineering Journal 2008; 143:124-132.

[16] Huang Y F, Kuan W H, Lo S L, Lin C F. Total recovery of resources and energy from rice straw using microwave-induced pyrolysis. Bioresource Technology 2008; 99:8252-8258.

[17] Urban D L, Anta Jr. M J. Study of the kinetics of sewage sludge pyrolysis using DSC and TGA. Fuel 1982;61:799.

[18] Zhai Y, Liu Q, Zeng G, Li C, Yang, Li S. Experimental study on the characteristics of sewage sludge pyrolysis under the low temperature conditions. Environmental Engineering Science 2008;25:8.

[19] Rutheven D M, Shamsuzaman, F, Kanebel K S. Pressure swing adsorption. First edition. New York: VCH Publishers, Inc.;1994.

[20] Nam G-M, Jeong B-M, Kang S-H,Lee B-K, Choi D-K. Equilibrium isotherms of CH_4, C_2H_6, N_2 and H_2 on zeolite 5A using a static volumetric method. J Chem Eng Data 2005;50:72-76.

[21] Jeong B-M, Ahn E-S, Yun J-H, Lee C-H, Choi D-K. Ternary adsorption equilibrium of $H_2/CH_4/C_2H_4$ on activated carbon. Separation and purification Technology 2007;55:335-342.

[22] Yang J, Han S, Cho C, Lee C-H, Lee H. Bulk separation of hydrogen mixtures by one-column PSA process. Separation Technology 1995;5:239-249.

[23] Zheng D-X, Xie Z-J, Fan Z. Prediction of breakthrough curves of the oxygen-nitrogen co-adsorption system on molecular sieves. Gas Separation & Purification 1988;2.

[24] Nikolic D, Giovanoglou A, Georgiadis M C, Kikkinedes S E. Modelling and simulation of multiple-bed pressure swing adsorption processes. Proceedings of the 17th European symposium on computer aided process engineering. Bucharest Romania, 27th-30th May, 2007.

[25] Yang S-I, Park J-Y, Choi D-K, Kim S-H. Effects of the residence time in four-bed pressure swing adsorption process. Separation Science and Technology 2009;44:1023-1044.

[26] Hideki M. Improved purge step in pressure swing adsorption for CO purification. Adsorption 2005;11:625-630.

[27] Siew Wah C, Mayuresh V K, Shivaji S. Rapid pressure swing adsorption for the reduction of bed size factor of medical oxygen concentrator. Industrial & Engineering Chemistry Research 2011;50:8703-8710.

[28] Cavenati S, Grande C A, Rodrigues A E. Separation of $CH_4/CO_2/N_2$ mixtures by layered pressure swing adsorption for upgrade of natural gas. Chemical Engineering Science 2006;61:3893-3906.

[29] Qinghong Z, Jincan K, Ye W. Development of novel catalysts for Fischer-Tropsch synthesis: Tuning the product selectivity. ChemCatChem 2010;2:1030-1058.

[30] Botes F G, Böhringer W. The addition of HZSM-5 to the Fischer-Tropsch process for improved gasoline production. Applied Catalysis A: General 2004;267:217-225.

[31] Pinna F. Supported metal catalysts preparation. Catalysis Today 1998;41:129-137.

[32] Soled S L, Iglesia E, Fiato R A, Baumgartner J E, Vroman H, Miseo S. Control of metal dispersion and structure by changes in the solid-chemistry of supported cobalt Fischer-Tropsch catalysts. Topics in Catalysis 2003;26:1-4.

[33] Andrei Y K, Wei C, Pascal F. Advances in the development of novel cobalt Fischer-Tropsch catalysts for synthesis of long-chain hydrocarbons and clean fuels. Chem Rev 2007;107:1692-1744.

[34] Jorhimurugesan K, Gangwal S K. Titania-supported bimetallic catalysts combined with HZSM-5 for Fischer-Tropsch synthesis. Ind Eng Chem Res 1998;37(4):1181-1188.

[35] Sundaram N, Wankat P C. Pressure drop effects in the pressurization and blowdown steps of pressure swing adsorption. Chem Eng Sci 1998;43:123.

[36] Yang S-I, Park J-Y, Choi D-K, Kim S-H. Effects of the residence time in four-bed pressure swing adsorption process. Separation Science and Technology 2009;44:1023-1044.

[37] Stocker J, Wysall M, Anterp, Miller G. Q. 30 years of PSA technology for hydrogen purification. A technical report. UOP LLC, 1998.

[38] Dantas T L P, Luna F M T, Silva Jr. I J, Torres A E B, de Azevedo D C S, Rodrigues A E, Moreira Regina F P M. Carbon dioxide-nitrogen separation through pressure swing adsorption. Chemical Engineering Journal 2011;172:698-704.

[39] Jacobs G, Das T D, Yongqing Z, Jinlin L. Fischer-Tropsch synthesis: support, loading and promoter effects on the reducibility of cobalt catalysts. Applied Catalysis A: General 2002;233:263-281.

[40] Kim C-U, Kim Y-S, Chae H-J, Jeong K-E. Effect of cobalt catalyst type and reaction medium on Fischer-Tropsch synthesis. Korean J Chem Eng 2010;27(3):777-784.

[41] Kolesnichenko N V, Kitae L E, Bukina Z M, Markova N A. Synthesis of gasoline from syngas via dimethyl ether. Kinetics and Catalysis. 2007;48(6):789-793.

[42] Patterson P M, Das T K, Davis B H. Carbon monoxide hydrogenation over molybdenum and tungsten carbides. Applied Catalysis A: General 2003;251:449-455.

[43] Bhattacharyya K G, Talukdar A K. Catalysis in petroleum and petrochemical industries. First edition. New Delhi: Narosa Publishing House Pvt. Ltd; 2005.

[44] Campbell I M. Biomass, catalysts and liquid fuels. First edition. Exeter, Devon, Great Britain: Wheaton and Sons Ltd;1983.

[45] Wood B R, Reimer J A, Bell A T. Studies of N_2O adsorption and decomposition on Fe-ZSM-5. Journal of Catalysis. 2002;209:151-158.

[46] Dadong S, Xiangke W, Qiaohui F. Photocatalytic reduction of Cr(VI) to Cr(III) in a solution containing ZnO or ZSM-5 zeolite using oxalate as model organic compound in the environment. Microporous Materials 2009;117:243-246.

[47] Noritatsu T, Yoshiharu Y, Keisuke M, Kaoru J. Three-component hybrid catalyst for direct synthesis of isoparaffin via modified Fischer-Tropsch synthesis. Catalysis Communications 2003;4:108-111.

[48] Scott Fogler H. Elements of Chemical Reactions Engineering. Fourth edition. Upper Saddle River, New Jersey: Prentice Hall Publishing Co.; 2005.

[49] Boateng Akwasi A, Daugard Daren E, Golberg Neil M, Hicks B K. Bench-scale fluidized-bed pyrolysis of switchgrass for bio-oil production. Ind Eng Chem Res 2007;46:1891-1897.

[50] Jay Chen. Biomass Conversion to Renewable Energy Processes. First edition. Boca Raton:Taylor and Francis Group;2010.

[51] Montgomery Douglas C. Design and Analysis of Experiments. Seventh edition. Hoboken, New Jersey: Wiley & Sons Inc. (Asia) Pte Ltd;2009.

[52] Perry R H, Greeen D W, Maloney J O. Perry's Chemical Engineers' Handbook. Sixth edition. New York: McGraw-Hill; 1984.

[53] Choi Y, Stenger H G. Water gas shift reaction kinetics and reactor modeling for fuel cell hydrogen. Journal of Power Sources 2003;124:432-439.

APPENDIX

Raw Data

Table A 1:: Temperature, feeding rate and syngas composition for sludge pyrolysis

run #	temperature ^{o}C	feed rate kg/min	H_2 comp. v/v %	CH_4 comp. v/v %	CO comp. v/v %
1	730	0.29	44.1	20.1	28.4
2	730	0.29	44.8	19.2	28.1
3	730	0.29	37.8	17.6	24.2
4	730	0.37	42.7	18.3	23.5
5	730	0.37	45.3	19.6	27.4
6	730	0.37	41.8	19.9	25.7
7	770	0.29	44.8	20.6	31.8
8	770	0.29	45.3	20.3	32.1
9	770	0.29	46.5	17.7	30.6
10	770	0.37	41.8	19.6	29.9
11	770	0.37	46.5	21.1	31.6
12	770	0.37	43.2	20.8	30.3
13	750	0.33	44.3	19.6	27.6
14	750	0.33	48.3	21	32.2
15	750	0.33	43.2	20.1	28.7
16	630	0.33	20.2	13.7	26.4
17	680	0.33	30.0	14.5	25.4
18	680	0.33	27.2	14.5	22.5
19	630	0.33	26.7	11.5	21.3
20	680	0.33	35.8	17.5	29.9
21	630	0.33	19.7	10.4	20.9

Table A 2:: Summary raw data from sludge pyrolysis

run	Temp (cel)	feed rate (rpm)	sludge fed (g)	bottle weight (g)	bottle + bio-oil (g)	Char (g)	unpyrolyzed (g)	Pyrolyzed (g)
1	730	2.6	2971	4150.4	4177.6	929.9	998	1973.2
2	770	3.4	3425	4150.4	4151.4	1292.8	590	2835
3	730	3.4	2926	4150.4	4218.5	1179.4	612	2313
4	730	2.6	2971	4150.4	4150.4	1043.3	839	2131
5	770	2.6	2971	4150.4	4150.4	997.9	794	2109
6	770	3.4	3062	4150.4	4154.9	1020.6	635	2200
7	730	3.4	2903	4150.4	4159.5	1043.3	748	2109
8	730	2.6	2812	4150.4	4218.5	997.9	612	2358
9	750	3.0	2971	4150.4	4164.1	1043.3	1066	1905
10	750	3.0	3062	4150.4	4159.5	1111.3	862	2200
11	770	2.6	2903	4150.4	4150.4	1043.3	839	2063
12	770	2.6	2812	4150.4	4150.4	997.9	726	2086
13	730	3.4	2722	4150.4	4150.4	1020.6	635	2086
14	770	3.4	2722	4150.4	4150.4	952.6	885	1837.1
15	750	3	2722	4150.4	4150.4	1043.3	590	2131.9
16	630	3	2948	4422.6	4898.8	1020.6	499	2449.4
17	680	3	2948	4422.6	4694.9	884.5	975	1973.2
18	680	3	2722	4422.6	4694.7	825.6	318	2404.1
19	630	3	2268	4422.6	4604.0	1066.0	136	2131.9
20	680	3	2495	4422.6	4581.4	929.9	318	2177.3
21	630	3	2563	4422.6	4898.9	907.2	318	2245.3

Table A 3:: Conversion factors($\times 10^{-3}$) used in the one-point calibration measurements of gaseous hydrocarbons

methane	ethylene	Ethane	propylene	propane	1-butene	n-butane
13.22	6.65	6.65	4.54	4.54	3.45	3.47
cis-2-butene	1 pentene	n pentane	iso pentane	hexene	n hexane	
3.43	3.46	3.40	3.39	3.40	2.9	

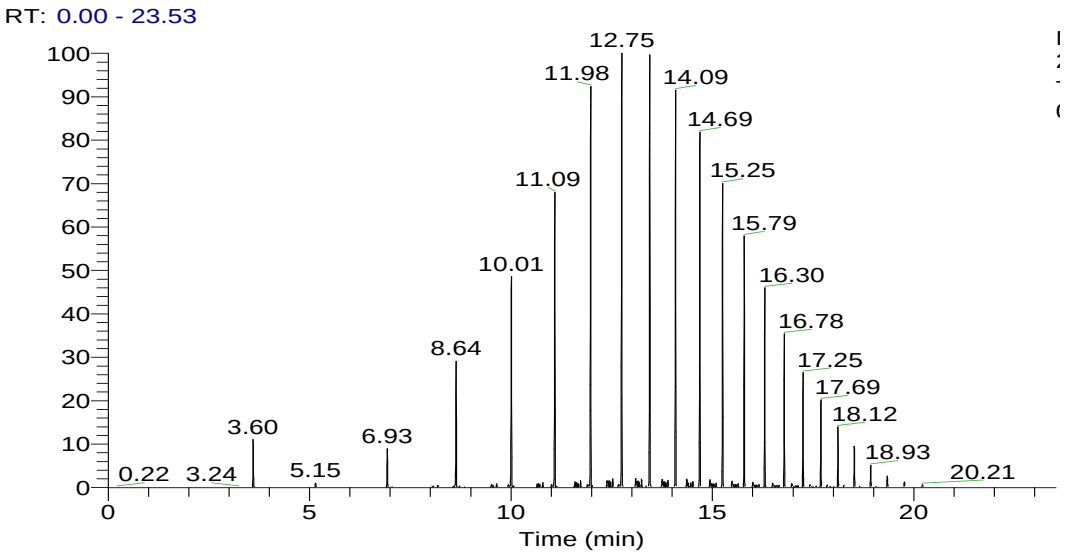

Table A 4:: GCMS hydrocarbons chromatogram for sample at 13.6 atm and 250 ^{o}C

Table A 5:: Carbon number and liquid hydrocarbon nomenclature (13.6 atm, 250 ^{o}C)

C #	nomenclature	C#	nomenclature
6	hexane	9	4 methyl octane
7	2 methyl hexane		3 methyl octane
	3 methyl hexane		cis-2-nonene
	heptane		trans-4-nonene
	cis-3-heptene		nonane
	2 heptene		2-nonene
8	2 methyl heptane	10	2 ethyl octane
	4 methyl heptane		5 methyl nonane
	3 methyl heptane		2 methyl nonane
	2-octene		4 ethyl octane
	cis-3-octene		cis-2-decene
	octane		1-decene
	2-octene		trans-4-decene
	cis-3-octene		2-decene

Table A 5 continued:: Carbon number and liquid hydrocarbon nomenclature (13.6 atm, 250 ^{o}C)

C #	nomenclature	C#	nomenclature
11	cis-5-undecene	14	4 methyl tridecane
	4 methyl 1-decene		5 methyl tridecane
	5 methyl decane		2 methyl tridecane
	4 methyl decane		3 methyl tridecane
	2 methyl decane		3 methyl tridecane
	3 methyl decane		cis-4-tetra decene
	5 undecene		1-tetradecene
	undecene	15	2,5 dimethyl tridecane
	2 undecene		5 methyl tetradecane
12	4 methyl 1-undecene		4 methyl tetradecane
	dodecane		3 methyl tetradecane
	2,3 dimethly decane		1 pentadecene
	3 methyl undecane		pentadecane
	cis-3-dodecene	16	7 methyl pentadecane
	3 dodecene		5 methyl pentadecane
	dodecane		4,11 dimethyl tetradecane
	2 dodecene		2 methyl pentadecane
13	5 tridecene		3 methyl pentadecane
	2,6 dimethyl undecane		1 hexadecene
	5,1 methyll undecane		hexadecane
	4 methyl dodecane	17	7 methyl hexadecane
	2,3 dimethly undecane		2,6,10 trimethyl tetradecane
	3 methyl dodecane		4 methyl hexadecane
	6 tridecene		3 methyl hexadecane
	tridecene		heptadecane
	1 tridecene	18	8 methyl heptadecane

Table A 5 continued:: Carbon number and liquid hydrocarbon nomenclature (13.6 atm, 250 ^{o}C)

C#	nomenclature	C#	nomenclature
18	2,6,10 trimethyl tetradecane	22	10 methyl heneicosane
	4 methyl hexadecane		docosane
	Octadecane	23	9 hexyl heptadecane
19	2,6 dimethyl heptadecane		Tricosane
	5 methyl octadecane	24	2 methyl tricosane
	4 methyl octadecane		tetracosane
	2,3 dimethyl heptadecane	25	9 octyl heptadecane
	3 ethyl octadecane		2,6,10,14,18 pentamethyl eicosane
	Nonadecane	26	Hexacosane
20	9 methyl nonadecane	27	heptacosane
	5 butyl hexadecane	28	octacosane
	4 methyl nonadecane	29	nonacosane
	eicosane	30	tricosane
21	10 methyl eicosane		
	8 hexyl pentadecane		
	2 methyl eicosane		
	3 methyl eicosane		
	heneicosane		

Table A 6:: Carbon number and liquid hydrocarbon nomenclature (10 atm ,250 ^{o}C)

C #	nomenclature	C#	nomenclature
6	hexane	10	2,3 dimethyl decane
7	2,4 dimethyl pentane	11	5 methyl decane
	3 methyl hexane		2 methyl decane
	heptane		3 methyl decane
8	2 methyl heptane		trans- 5- undecene
	2methyl heptane		undecane
	3 ethyl hexane		5 undecene
	octane		cis- 3-undecene
	2-octene	12	6 methyl undecane
9	4 methyl octane		2,3 dimethyl decane
	3 methyl octane		3 methyl undecane
	cis 4 nonene		3 dodecene
	nonane		trans- 3- dodecene
	cis 2 nonene		dodecane
	4 nonene		trans- 3- dodecene
10	4 methyl octane		trans-2- dodecene
	5 methyl nonane	13	2,3 dimethyl undecane
	2 propyl heptane		5-(1-methyl propyl)nonane
	3 ethyl, 2 methyl heptane		2,3 dimethyl undecane
	3 methyl nonane		4 methyl dodecane
	cis-3-decene		3 methyl dodecane
	cis-4-decene		6 tridecene
	decane		6 tridecene
	cis-2-decene		tridecane
	3 ethyl octane		1 tridecene
	2,3 dimethyl decane		

Table A 6 continued:: carbon number and liquid hydrocarbon nomenclature (10 atm ,250 ^{o}C)

C #	nomenclature	C#	nomenclature
14	2,5 dimethyl dodecane	17	2,6,10 trimethyl tetradecane
	5 methyl tridecane		4 methyl hexadecane
	4 methyl tridecane		3 methyl hexadecane
	2,3 dimethyl dodecane		2, methyl E-7 hexadecene
	3 methyl tridecane		heptadecane
	5 tetradecene	18	7 methyl heptadecane
	cis- 4- tetradecene		2,6,10 trimethyl heptadecane
	tetradecane		4 methyl heptadecane
	1 tetradecene		3 methyl heptadecane
15	2,5 dimethyl tridecane		1 octadecene
	5 methyl tetradecane		octadecane
	4 methyl tetradecane	19	2,6 dimethyl heptadecane
	2 methyl tetradecane		5 methyl octadecane
	3 methyl tetradecane		2,3 dimethyl heptadecane
	1 pentadecene		3 methyl octadecane
	pentadecane		nonadecane
16	7 methyl pentadecane	20	9 methyl nonadecane
	5 methyl pentadecane		5 butyl hexadecane
	4,11 dimethyl tetra decane		4 methyl nonadecane
	2 methyl pentadecane		2 methyl nonadecane
	3 methyl pentadecane		3 methyl nonadecane
	1 hexadecene		ecosane
	cis-3 hexadecene		10 methyl eicosane
	hexane	21	5,15 dimethyl nondecane
	7 methyl hexadecane		2,3 dimethyl nonadecane

Table A 6 continued:: carbon number and liquid hydrocarbon nomenclature (10 atm ,250 ^{o}C)

C #	nomenclature	C#	nomenclature
21	2, 3 dimethyl nonadecane	24	2 methyl tricosane
	3 methyl eicosane		3 methyl tricosane
	heneicocane		tetracosane
	docosane	25	9 octyl heptadecane
22	5 methyl heneicosane		pentadecane
	3 methyl heneicosane	26	11, (1-ethylpropyl) heneicosane
	docosane	27	heptacosane
23	9 hexyl heptadecane	28	5-octyl eicosane
	4 methyl docosane	29	nonacosane
	tricosane		

VITA

Name:	Eliasu Azinyui Teiseh
Address:	Department of Biological and Agricultural Engineering, 2117, TAMU, College Station, Texas,77843.
Email Address:	eliasy1@yahoo.com
Education:	B.S., Environmental Science/Chemical Processing Technology, University of Buea, 2001 M.S., Environmental Engineering, University of Wyoming, 2007 Ph.D., Biological & Agricultural Engineering, Texas A&M University, 2012